Revision 1

A shallow salt pond analog for aqueous alteration on ancient Mars: Spectroscopy, mineralogy, and geochemistry of sediments from Antarctica's Dry Valleys

ZACHARY F. M. BURTON[1,2,*], JANICE L. BISHOP[2,3], PETER A. J. ENGLERT[4], ANNA SZYNKIEWICZ[5], CHRISTIAN KOEBERL[6], PRZEMYSLAW DERA[4], WARREN MCKENZIE[4], AND EVERETT K. GIBSON[7]

[1]Department of Geological Sciences, Stanford University, Stanford, California 94305, U.S.A.

[2]Carl Sagan Center, The SETI Institute, Mountain View, California 94043, U.S.A.

[3]NASA Ames Research Center, Moffett Field, California 94035, U.S.A.

[4]Hawai'i Institute of Geophysics and Planetology, University of Hawai'i at Mānoa, Honolulu, Hawaii 96822, U.S.A.

[5]Department of Earth and Planetary Sciences, University of Tennessee, Knoxville, Tennessee 37996, U.S.A.

[6]Department of Lithospheric Research, University of Vienna, Althanstrasse 14, A-1090 Vienna, Austria

[7]NASA Johnson Space Center, Houston, Texas 77058, U.S.A.

* E-mail: zburton@stanford.edu

ABSTRACT

Understanding past and present aqueous activity on Mars is critical to constraining martian aqueous geochemistry and habitability, and to searching for life on Mars. Assemblages of minerals observed at or near the martian surface include phyllosilicates, sulfates, iron oxides/hydroxides, and chlorides, all of which are indicative of a complex history of aqueous activity and alteration in the martian past. Furthermore, features observed on parts of the martian surface suggest present-day activity of subsurface brines and at least transient liquid water. Terrestrial analogs for younger and colder (Hesperian–Amazonian) martian geologic and climatic conditions are available in the McMurdo Dry Valleys (MDV) of Antarctica and provide opportunities for improved understanding of more recent aqueous activity on Mars. Here, we study the VXE-6 intermittent brine pond site from Wright Valley in the MDV region, and use coordinated spectroscopy, X-ray diffraction, and elemental analyses to characterize the mineralogy and chemistry of surface sediments that have evolved in response to aqueous activity at this site. We find that brine pond activity results in mineral assemblages akin to aqueous alteration products associated with younger sites on Mars. In particular, surficial chlorides, a transition layer of poorly crystalline aluminosilicates and iron oxides/hydroxides, and a deeper gypsum-rich interval within the upper 10 cm of sediment are closely related at this Antarctic brine pond site. Activity of the Antarctic brine pond and associated mineral formation presents a process analog for chemical alteration on the martian surface during episodes of transient liquid water activity during the late Hesperian and/or more recently. Our results provide a relevant example of how aqueous activity in a cold and dry Mars-like climate may explain the co-occurrence of chlorides, clays, iron oxides/hydroxides, and sulfates observed on Mars.

Keywords: Mars; McMurdo Dry Valleys, Antarctica; sulfates; chlorides; clays; brine pond; aqueous alteration; geochemistry; spectroscopy; Earth Analogs for Martian Geological Materials and Processes

INTRODUCTION

Understanding the history of liquid water on Mars is central to constraining that planet's geochemical and possible biological evolution. Liquid water appears to have been present in the martian past, based on both mineralogical evidence (e.g., Carr, 1987, 1996; Squyres et al., 2004; Mustard et al., 2008; Murchie et al., 2009, 2019; Ehlmann and Edwards, 2014; Carter et al. 2015) and geomorphological features such as valley networks, dendritic channels, and deltas that indicate frequent flowing water and fluvial erosion on early Mars (e.g., Craddock and Howard, 2002; Ansan et al., 2008; Fassett and Head, 2011), but liquid water is not currently stable on the surface (Haberle et al., 2001; Wordsworth, 2016).

Evidence for past aqueous activity on Mars includes the identification of sulfates (including gypsum, kieserite, and polyhydrated Fe and Mg sulfates, e.g., Langevin et al., 2005; Murchie et al., 2009), hydrated phyllosilicates (including smectite, mica, chlorite, and kaolinite, e.g., Bibring et al., 2005; Poulet et al., 2005; Bishop et al., 2008; Ehlmann et al., 2009), and chlorides (Osterloo et al., 2008). Phyllosilicates indicate a complex history of aqueous alteration on early Mars (e.g., Murchie et al., 2009; Carter et al., 2015), with associations of phyllosilicates, sulfates, and other minerals suggesting variable aqueous environments on the martian surface (Bishop, 2018). In particular, colder environments support formation of poorly crystalline aluminosilicates rather than crystalline phyllosilicates (Bishop et al., 2018). These poorly crystalline materials are

abundant across the surface of Mars (Rampe et al., 2012), at the top of the clay profile in areas with abundant phyllosilicates (Bishop and Rampe, 2016) and in all of the samples investigated by the *Curiosity* rover's CheMin instrument at Gale crater (e.g., Blake et al., 2013; Bristow et al., 2018, 2021). Inferred formational processes for both sulfates and chlorides include evaporation from saline bodies of water (Langevin et al., 2005; Osterloo et al., 2008), which originated from ponding of surface runoff or groundwater upwelling (Osterloo et al., 2010; Hynek et al., 2015). Chlorides on Mars appear bright in color, and occur predominantly within topographic lows, further supporting an evaporitic origin (Osterloo et al., 2008). Some locations exhibit morphological evidence for mobilization and deposition of salts by near-surface waters (Glotch et al., 2010).

The study of terrestrial analogs provides a key tool in interpreting and constraining the mineralogical, aqueous, and geochemical history of Mars, and the McMurdo Dry Valley (MDV) region of Antarctica explored here has long served as a compelling analog for such processes (Anderson et al., 1972; Morris et al., 1972; Gibson et al., 1983). In general, the cold and xeric conditions of the MDV region provide a close analog for recent conditions on Mars (Bull, 1965; Thompson et al., 1971). Similarly, the geological setting of the MDV region, and in particular, the Don Juan Pond area, could be analogous to martian sedimentary and evaporite settings in that the MDV's Ferrar dolerite has a composition close to that of martian basalts, and in its weathered form can resemble martian regolith (McKelvey and Webb, 1962; Claridge and Campbell, 1984; Harvey, 2001). Although the high quartz content of much MDV sediment (McKelvey and Webb, 1962; Gibson et al., 1983; Nedell et al., 1987; Bishop et al., 1996) originating from other rock units (e.g., Beacon Supergroup, crystalline basement) is different from the chemistry of martian sediments (e.g., Clark, 1993; McSween, 2002; Velbel, 2012; McLennan et al., 2014; Vaniman et al., 2014;

Gellert and Yen, 2019), trends in the weathering of feldspar and pyroxene and precipitation of evaporites are similar to processes on Mars (e.g., Gibson et al., 1983; Wentworth et al., 2005; Phillips-Lander et al., 2019). Notably, chemical weathering of the local bedrock has been found to produce salts, sulfates, fine-grained ferric oxides/hydroxides, poorly crystalline aluminosilicates, and even minor amounts of phyllosilicates in some areas (Claridge, 1965; Ugolini and Anderson, 1973; Claridge and Campbell, 1984; Allen and Conca, 1991), and in general, chloride and sulfate salts are widespread in the surficial MDV sediments (Claridge, 1965; McCraw, 1967; Claridge and Campbell, 1977; Bockheim, 2002). Throughout the western region of Wright Valley, including its North and South forks, soils are characterized as Typic Haplorthels/Haploturbels (McLeod et al., 2009). Finally, though liquid water is scarce, unfrozen waters do occur in the form of brine ponds, lakes, and shallow groundwater in the MDV, providing a noteworthy example of the persistence of liquid water in harsh, Mars-like conditions (Harris, 1981; Harris and Cartwright, 1981; Dickson et al., 2013).

The observed mineral assemblages, brine geochemistry, cold and xeric conditions, and geological setting of the MDV region's Wright Valley, as well as relatively high solar radiation and relatively low magnetic fields, all combine to form an excellent analog for more recent conditions on Mars (Anderson et al., 1972; Morris et al., 1972; Gibson et al., 1983; Samarkin et al., 2010).

Here, we conduct spectroscopic, mineralogical, and geochemical analyses of sediment samples from the VXE-6 transient salt pond site near the Don Juan Pond in Wright Valley of the MDV in order to characterize sediment horizons that developed in response to the intermittent activity of this brine water system. The results are used to determine how such activity on or near the ancient martian surface may have influenced and resulted in the formation of observed sulfates, poorly crystalline aluminosilicates, iron oxides/hydroxides, and chlorides.

111

112 CLIMATIC AND GEOLOGIC SETTING OF THE MCMURDO DRY VALLEYS

113 Late Quaternary deglaciation has left the Wright Valley region ice-free (McKelvey and Webb,
114 1962; Hall et al., 1997), with much of the unconsolidated sediment on the basin floor likely of
115 glacial origin (Harris and Cartwright, 1981). The brine pond site studied here was named VXE-6
116 after the Navy helicopter squadron (VXE-6) tasked with Antarctic flights at the time this pond was
117 identified. The VXE-6 basin is bounded to the north and to the south by mountains made up of
118 orthoquartzite sandstones of the Devonian–Triassic Beacon Supergroup (Figs. 1a and 1b)
119 (Harrington, 1958; McKelvey and Webb, 1962; Shaw, 1962; Barrett et al., 1986). These mountains
120 are pervasively intruded by dikes of igneous Ferrar dolerite (Harrington, 1958; McKelvey and
121 Webb, 1962). The Jurassic Ferrar dolerite contains pyroxenes, plagioclase feldspar, variable
122 amounts of quartz-alkali feldspar intergrowths, and accessory minerals, but little olivine (Clarkson,
123 1981; Elliot et al., 1985; Barrett et al., 1986; Bédard et al., 2007).

124 Chemical weathering of Antarctic dolerite yields micaceous phyllosilicates, including Fe-rich clay
125 minerals and smectites such as authigenic montmorillonite, as well as amorphous material,
126 chlorite, uralite, a "brown micaceous mineral" (Clarkson, 1981), and salts including gypsum
127 (Claridge, 1965; Ugolini and Anderson, 1973; Claridge and Campbell, 1984; Elliot et al., 1985;
128 Allen and Conca, 1991). In general, sulfates, chlorides, and nitrates are widespread in Antarctic
129 sediments of the MDV, and their origins are inferred to include deposition of original marine salts
130 or aerosols as well as chemical weathering of volcanic material (Claridge, 1965; McCraw, 1967;
131 Claridge and Campbell, 1977; Bockheim, 2002; Szynkiewicz and Bishop, 2021; Szynkiewicz et
132 al., 2021).

Although chemical properties of sediment within Antarctic endorheic basins often vary widely, these basins (with relatively abundant amounts of moisture) are often characterized by elevated clay and salt contents (Campbell and Claridge, 1982). Notably, salt accumulations tend to occur at or near the ground surface (rather than as a deeper horizon, as seen in most other Antarctic sediment profiles) and clays are inferred to have mostly formed via weathering processes enhanced by the presence of moisture (Claridge, 1965; Campbell and Claridge, 1982).

CLIMATE, HISTORY OF WATER, AND MINERALOGY OF MARS

Orbiter- and rover-based mineralogical observations of the martian surface over the past two decades, paired with studies of Mars analog material, support the conclusion that the Noachian (~4.1–3.5 Ga) period of early Mars was characterized by episodically warm and wet conditions, whereas the succeeding Hesperian (~3.5–3.0 Ga) and Amazonian (~3.0–0 Ga) periods have been characterized by colder and drier conditions (e.g., Warner et al., 2010; Wordsworth, 2016; Bishop et al., 2018; Kite, 2019). Liquid water is inferred to have been stable on the martian surface during parts of the Noachian, but was limited to transient surface occurrence during the Hesperian and Amazonian (Bibring et al., 2006; Fassett and Head, 2008a,b; Tosca and Knoll, 2009; Bishop, 2018). However, sufficient water was present at Gale crater during the Hesperian to form ample smectite clays (e.g., Bristow et al., 2018, 2021; Rampe et al., 2020).

Mafic and ultramafic material and volcanic landforms typify much martian surface geology, and volcanism is inferred to have been an important and potentially still-active process throughout martian history (e.g., Greeley and Spudis, 1981; Wilson and Head, 1994; Hartmann et al., 1999; Hauber et al., 2011). The surface mineralogy of Mars is dominated by the occurrence of Fe-bearing

pyroxene, plagioclase feldspar, and olivine, but also includes substantial areas that have undergone heavy alteration (physical and/or chemical) or are covered by altered dust (Christensen et al., 2001; Bandfield, 2002; Bibring et al., 2005, 2006; Ehlmann and Edwards, 2014).

Trends in the temporal (stratigraphic) and spatial distribution of these alteration products—which include clay minerals, iron oxides/hydroxides, sulfates, and chlorides—have been used to discern the paleoclimate and history of liquid water at and near the martian surface. Alteration assemblages differ significantly through time, with Fe/Mg smectites globally widespread in outcrops of the Noachian age, Al phyllosilicates in the later Noachian and earlier Hesperian, sulfates and chlorides through most of the Hesperian, and sulfate-silica diagenetic/weathering assemblages starting in the Hesperian and into the Amazonian (e.g., Bibring et al., 2006; Ehlmann and Edwards, 2014; Murchie et al., 2019). Widespread clay minerals in the Noachian have been interpreted as an indicator of weathering, hydrothermal activity, and diagenesis in aqueous environments (Ehlmann and Edwards, 2014). Localized clays, sulfates, iron oxides/hydroxides, chlorides, and carbonates from the Noachian and Hesperian occur in interpreted paleolake deposits (Ehlmann and Edwards, 2014; Rampe et al., 2020). More localized occurrences of sulfates and silica in the late Hesperian to Amazonian suggest that, though rare, ground and surface waters have also occurred in recent martian history (Weitz et al., 2013; Ehlmann and Edwards, 2014).

METHODS

Samples

The sediments studied here were collected from the then-dry VXE-6 pond site by Everett Gibson during a 1980 field season that resulted in a study (Gibson et al., 1983) on silty tills and gravels of

Wright Valley's Prospect Mesa. The VXE-6 pond site (this study) is located ~15 km west of the Prospect Mesa site (the Gibson et al., 1983, study) and sits ~1 km east and upslope of hypersaline Don Juan Pond (Fig. 1). VXE-6 pond site sediments were collected both in the form of bulk ~200–500 g samples collected at various depths of a soil pit using a stainless steel spatula and in the form of a ~14-cm-deep, ~2-cm-wide core. Soil pit samples were collected at six depth intervals (0–1, 1–4, 4–7, 8–10, 12–15, and 20–24 cm) (Figs. 2a,b) down to the top of the permafrost, while the continuous core samples were available for one-cm intervals from 0–14 cm depth (Fig. 2c), as summarized in Table 1. Samples were shipped from Antarctica to the United States in a freezer and stored at NASA Johnson Space Center at −40 °C (as described for the Prospect Mesa samples examined by Gibson et al., 1983). Tubs containing the bulk soil pit samples were kept fully sealed and unopened until our 2018–2021 analytical work. Both sample sets were available for this study as sediment grains in their original form as collected in 1980 (Figs. 2a,c), while the soil pit samples were also available as finely-crushed particles prepared but not analyzed by Gibson following the 1980 field season (Fig. 2b) (note that these finely-crushed samples were only used for some of the spectroscopy work that we present herein).

X-ray diffraction

X-ray powder diffraction (XRD) analysis of soil pit samples was performed in 2021 at the University of Hawai'i at Mānoa. Bulk powders were prepared for analysis by grinding aliquots of the bulk, freshly opened soil pit samples in a McCrone micronizing XRD-mill for 1 hour at 10 Hz oscillating frequency. A thin layer of each sample was deposited on a silicon single crystal wafer zero-background holder, and XRD data were collected using a Bruker D8 Advance diffractometer (CuKα source operating at 40 mA and 40 kV in a parafocusing Bragg-Brentano mode) with a Lynxeye XE detector and 0.020 mm Ni filter inserted into the diffracted beam path. Phase

identification was performed using Bruker Diffrac.Eva software (version 4.2.0.14) with the ICDD PDF 4+ database (2021 edition) used as a reference for search-and-match. Rietveld refinement analysis was carried out using the Bruker data reduction program Diffrac.TOPAS (version 5).

Reflectance spectroscopy

Aliquots of the soil pit samples and core samples were freshly ground in 2018 and 2020, respectively, by carefully crushing the sediment grains and dry sieving the crushed product until all material passed through a <125 μm sieve (as described in Bishop et al., 2014a). To avoid over-grinding of the softer grains, crushed samples prepared in 2018 and 2020 were ground and sieved iteratively. Visible/near-infrared (VNIR) reflectance spectra of the coarse soil pit and core sediment grains in original form, of the finely-crushed soil pit particles prepared in 1983, and of the <125 μm soil pit sediment aliquots prepared in 2018 were measured under ambient conditions using an ASD FieldSpecPro spectrometer at the SETI Institute relative to Spectralon®. These spectra were obtained in order to compare the spectra of sample grains prepared at different times and ground in different ways.

Bidirectional reflectance spectra from 0.3–2.5 μm relative to Halon under ambient conditions and reflectance spectra from 1–50 μm relative to a rough gold standard were obtained under controlled dry conditions using a Nicolet FTIR instrument at the RELAB facility at Brown University (as detailed in previous work, e.g., Bishop et al., 2014a) for both finely-crushed soil pit particles prepared in 1983 and the <125 μm core sample aliquots prepared in 2020. The RELAB spectra were then spliced at ~1.2 μm and the longer wavelength Nicolet spectra were scaled to the shorter wavelength bidirectional spectra, enabling absolute reflectance values for spectra of samples without adsorbed water on grain surfaces.

222 **Elemental analyses**

223 Major element geochemical data were obtained via X-ray Fluorescence (XRF) at the Bureau
224 Veritas in Vancouver, Canada, in 2019 for the freshly prepared soil pit samples. Additional
225 elemental abundances, including those of the rare earth elements, were obtained using Instrumental
226 Neutron Activation Analysis (INAA) of the soil pit samples. INAA was conducted at the
227 University of Vienna. Further details on specific instrumentation, precision, and accuracy of INAA
228 are detailed in previous work by Koeberl and others (e.g., Koeberl, 1993; Mader and Koeberl,
229 2009).

230

231 **Sulfur analysis**

232 The $\delta^{34}S$ of oxidized and reduced S species in ~10 g aliquots taken from the bulk soil pit samples
233 was analyzed using a S sequential extraction (SSE) method in 2021. This technique allows for
234 separation of various S species (acid-soluble SO_4^{2-}, elemental S, acid-volatile and chromium-
235 reducible sulfides) for quantitative and $\delta^{34}S$ analyses (e.g., as detailed in Mayer and Krouse, 2004).
236 The S isotope composition ($\delta^{34}S$) of $BaSO_4$ and Ag_2S precipitated during the SSE process was
237 measured using a Costech elemental analyzer (EA) coupled with a Delta Plus XL IRMS at the
238 University of Tennessee, and the O isotope composition ($\delta^{18}O$) of $BaSO_4$ was measured using a
239 Thermo Finnigan TC/EA. The analytical precision for both $\delta^{34}S$ and $\delta^{18}O$ of $BaSO_4$ was <0.3‰.

240

241 **RESULTS**

242 **X-ray diffraction**

Results of XRD analysis indicate distinct changes in mineralogy with depth (Fig. 3; Table 2). At the 4–7 cm soil pit sample depth, abundances of albite, anorthite, quartz, and diopside are markedly lower than at all other sample depths (at least ~36% lower for albite, ~21% lower for anorthite, ~33% lower for quartz, and ~28% lower for diopside), with the exception of the albite abundance at the 20–24 cm depth (which is nonetheless 15% higher than the albite abundance at 4–7 cm) (Fig. 3; Table 2). Conversely, the abundance of phlogopite/muscovite and clinochlore is significantly higher at the 4–7 cm depth than at any other sample depth (Fig. 3; Table 2). The abundance of phlogopite/muscovite in the 4–7 cm depth soil pit sample is 30.7 wt%, while it is just 0.35 wt% at the 1–4 cm depth and absent at all other depths (Table 2). Clinochlore abundance is 8.68 wt% at the 4–7 cm depth, is at least ~57% lower in abundance in the 0–4 cm depth samples, and is absent from the 8–10, 12–15, and 20–24 cm depth samples (Table 2). Gypsum and bassanite are essentially found only in the 8–10 and 12–15 cm depth samples, and abundances are notably higher at the 8–10 cm depth than at the 12–15 cm depth, with gypsum abundances of 0.76 wt%, 11.20 wt%, and 5.19 wt% for the 0–1, 8–10, and 12–15 cm sample depths, respectively, and bassanite abundances of 3.74 wt% and 0.44 wt% at the 8–10 and 12–15 cm sample depths, respectively (Figs. 3 and 4, Table 2). Abundance of amphibole is somewhat lower (~17–45% lower) in the 0–7 cm depth samples than at the 8–10, 12–15, and 20–24 cm depth samples (Table 2).

Reflectance spectroscopy

General spectroscopic characteristics. Reflectance spectra in the region 0.3–5 μm for six soil pit sample aliquots and for ten core samples are shown in Figs. 5 and 6, respectively, while spectra of the core samples in the region 5–50 μm (plotted in wavenumber; 200–2000 cm^{-1}) are shown in Fig. 7. The spectroscopy data largely corroborate the data obtained via XRD analysis (Figs. 3 and

4; Table 2). These spectra illustrate the presence of quartz, pyroxene, gypsum, and aluminosilicates observed in sediments from the MDV in previous studies (e.g., Bishop et al., 1996, 2001, 2003, 2014). The VNIR spectra from the soil pit and core samples include features due to pyroxene, gypsum, iron oxides/hydroxides, and additional hydrated phases. The dominant band near 1 μm is due to pyroxene, but shifts in the shape and band center near 0.9 μm are consistent with iron oxides and hydroxides. This is especially observed in spectra of soil pit sample JB1102 from 4–7 cm depth (Fig. 5) and core samples JB1309 from 6–7 cm depth and JB1310 from 7–8 cm depth (Fig. 6). Gypsum bands (e.g., Bishop et al., 2014b) near 1.45–1.53 (triplet), 1.75, 1.94, 2.22, 2.5, 4.75, and 4.85 μm appear strongest in spectra of soil pit sample JB1104 from 8–10 cm depth (Fig. 5) and core samples JB1311 from 8–9 cm depth and JB1312 from 9–10 cm depth (Fig 5). Spectra of other samples include bands near 4.75 and 4.85 μm with the stronger band near 4.85 μm, which is more consistent with anhydrite.

Strong water bands are also observed near 1.92 and 2.9–3.0 μm in most spectra. Variations in the shape and band position of these water bands are shown with core sample depth in Figure 6. The spectrum of the sample at 0–1 cm depth (JB1303) has the weakest hydration bands, consistent with exposure to the dry surface environment. The water band near 1.92 μm was quantified for the soil pit samples, indicating the highest normalized H_2O absorptions for the soil pit sample from 8–10 cm depth (JB1103), and lowest absorptions for the samples from 4–7 cm (JB1102) and 20–24 cm (JB1105) depths (Fig. 8).

Spectra of the soil pit sample from 4–7 cm depth (JB1102) and core samples from 3–6 cm depths (JB1306, JB1307, and JB1308) include stronger and narrower bands near 1.41, 1.93, and 2.20 μm that are not consistent with smectites (Bishop et al., 2008) or allophane (Bishop et al., 2013), but are attributed to poorly crystalline aluminosilicate materials and may be proto-clay phases. These

This is the peer-reviewed, final accepted version for American Mineralogist, published by the Mineralogical Society of America.
The published version is subject to change. Cite as Authors (Year) Title. American Mineralogist, in press.
DOI: https://doi.org/10.2138/am-2022-8381. http://www.minsocam.org/

four spectra also have a similar band shape near 2.8–3 μm that is due to overlapping OH and H_2O stretching bands from Al-OH, Si-OH, and water bands in a hydrous component.

Spectra of samples JB1304 (1–2 cm), JB1309 (6–7 cm) and JB1310 (7–8 cm) have broader features near 1.41, 1.94, and 2.92–2.94 μm that are consistent with halite (Fig. 6) or related hydrated salts. The triplet feature near 1.45–1.53 μm and strong band at 1.94 μm in spectra of samples JB1311 (8–9 cm) and JB1312 (9–10 cm) are distinct from the others and remarkably characteristic of gypsum (Fig. 6).

The spectra of JB1303 (0–1 cm) and JB1305 (2–3 cm) also have a band at 2.36 μm (Fig. 6), characteristic of the OH combination (stretch plus bend) band for OH bound to Fe^{2+} and Mg cations that is consistent with Fe/Mg-rich mica or actinolite. These two spectra also have a narrower band centered near 2.9 μm due to the OH stretching vibration.

The mid-IR reflectance spectra are dominated by features characteristic of quartz (Fig. 7). The primary quartz Si-O stretching band at 1225 cm^{-1} shifts towards lower wavenumbers for mixtures of quartz with gypsum (Fig. 7b). The primary gypsum S-O stretching band occurs near 1200 cm^{-1} and additional gypsum bands occur near 680 and 610 cm^{-1} (Bishop et al., 2014b). These features are observed in spectra of samples JB1311 (8–9 cm) and JB1312 (9–10 cm).

Differences due to sample preparation. Generally, reflectance spectra differ in absolute reflectance value according to particle size (Fig. 9) and differ in water band characteristics according to moisture conditions during analysis (Fig. 10), but overall display similar spectral signatures and yield consistent spectral results regardless of sample preparation or moisture environment.

Finer-grained material analyzed here, both from 1983 and 2018 preparations, show systematically higher reflectance values than spectra of the coarse original sediment grains (Fig. 9). Similarly, the finest-grained particles prepared in 1983 show systematically higher reflectance values than the fine-grained but slightly coarser <125 μm sediment aliquots prepared in 2018 (Fig. 9). Nonetheless, aside from these absolute reflectance values, the observed spectral features are consistent regardless of method of sample preparation.

Differences due to moisture environment. In a comparison of spectra obtained from the finely-crushed sediment samples prepared in 1983 under different moisture environments (ambient vs. dry), water bands near 1.4 and 1.9 μm are found to vary greatly (Fig. 10). Measurements made under ambient conditions yielded more pronounced, deeper water bands than measurements made under controlled dry conditions (Fig. 10) that is attributed to adsorbed water. This is characteristic of poorly crystalline aluminosilicates including allophane (e.g., Bishop et al., 2013) that readily adsorb water from the environment due to the fine particle size and high surface area. Notably, the sediment sample from 8–10 cm depth shows the least variation with changing moisture environment (Fig. 10). Aside from water band characteristics, observed spectral features are consistent regardless of the moisture environment present during spectral analysis.

Elemental analyses

INAA elemental abundance data reveal clear trends with depth (Fig. 11; Table 3). Abundances of the elements U, Cs, Fe, Th, Co, Zn, Rb, Zr, Ba, Sr, and Sc are effectively equal for most soil pit sample depths. However, the abundances of these elements are significantly elevated at the 4–7 cm soil pit sample depth (~62% higher than at any other depth for K, ~144% for U, ~260% for Cs,

~71% for Fe, ~126% for Th, ~51% for Co, ~67% for Zn, ~119% for Rb, ~16% for Zr, ~8% for Ba, ~26% for Sr, ~9% for Sc, ~38% for Ta) (Fig. 11; Table 3).

Results from rare earth elemental abundance data reveal similar trends, whereby the soil pit sample from 4–7 cm depth contains systematically higher abundances of all rare earth elements in comparison with other sample depths (Fig. 12; Table 4). At the 4–7 cm depth, concentration of La is ~48% higher than at any other depth, Ce is ~36% higher, Nd is ~40% higher, Sm is ~47% higher, Eu is ~21% higher, Gd is ~26% higher, Tb is ~39% higher, Tm is ~15% higher, Yb is ~38% higher, and Lu is ~42% higher (Table 4).

XRF major element chemistry data similarly indicate that the 4–7 cm depth interval is a horizon of elevated chemical abundance of Al, Fe, Mg, and K (Fig. 13; Table 5). At the 4–7 cm soil pit sample depth, Al_2O_3, Fe_2O_3, MgO, and K_2O values are all markedly elevated above (~19–79% higher than) those values for other sample depths, while SiO_2 at the 4–7 cm depth is ~18–31% lower than at any other sample depths (Fig. 13; Table 5). Abundances of CaO and SO_3 are significantly elevated at the 8–10 cm soil pit sample interval (whereby CaO at 8–10 cm is at least ~98% higher than that at 0–4 cm and at least ~50% higher than at 4–7 or 20–24 cm depths, and whereby SO_3 at 8–10 cm is >1200% higher than at 0–7 cm and ~350% higher than at 20–24 cm), and are somewhat elevated at the 12–15 cm depth interval (Fig. 13; Table 5). Abundance of Na_2O at surficial depths (0–4 cm) is ~18–24% higher than at 4–10 cm depths (2.19 and 2.11 wt% at 0–1 and 1–4 cm depths versus 1.76 and 1.79 wt% at 4–7 and 8–10 cm depths), while Na_2O abundance at greater depth (2.05 wt% at 20–24 cm) is comparable to surficial levels.

Sulfur analysis

353 Results of sulfur sequential extraction reveal traces of bedrock sulfides (<0.002 wt% S) in the
354 South Fork catchment with a narrow range of $\delta^{34}S$ of +1.0 to +3.0 ‰ (Fig. 14) consistent with an
355 igneous origin from detrital pyrite derived from the Ferrar dolerite (Hagen, 1988). There is little
356 variation of $\delta^{34}S$ and $\delta^{18}O$ of sulfate with depth (+15.8 to +16.7 ‰ and -8.9 to -7.2 ‰, respectively;
357 Table 6). Both the sulfate from the VXE-6 pond site investigated here and from other sediments
358 of the MDV investigated by Bao and Marchant (2006) show a distinctive, positive linear
359 relationship of $\delta^{34}S$ vs. $\delta^{18}O$, following the mixing line for seawater aerosol- and bedrock sulfide-
360 derived sulfate (Fig. 14). Thus, quantitative contributions of the bedrock-sourced sulfate in VXE-
361 6 sediments can be estimated via sulfur isotope mass balance using the equation:

362 $$\delta^{34}S_{\text{soil sulfate}} = x \cdot \delta^{34}S_{\text{sulfide-derived sulfate}} + (1-x) \cdot \delta^{34}S_{\text{marine sulfate}}$$

363 where x is an input from sulfide-derived sulfate.

364 Accordingly, up to ~20% of sulfate in the VXE-6 site sediments is derived from bedrock
365 weathering of the Ferrar dolerite (and/or basement complex), while the remaining ~80% is of
366 marine origin delivered via atmospheric deposition and/or from local sources (e.g., brines,
367 dissolution of sedimentary rocks). Generally, our estimates fall within the range of sulfide-derived
368 sulfate contributions suggested by Bao and Marchant (2006).

369 Microbial sulfate reduction has been observed in modern lakes of the MDV (Bishop et al., 2001,
370 2003) and Ace Lake of East Antarctica (Sun et al., 2015), and inferred for older lake deposits near
371 the Lewis Cliff Ice Tongue (Sun et al., 2015). The relatively small, shallow VXE-6 pond was dry
372 at the time of sampling, but could potentially have supported microbial sulfate reduction under
373 past wet conditions. Notably, the $\delta^{34}S$ of VXE-6 sediments was shifted (increased) by ~3‰ from
374 the mixing line (Fig. 14), potentially suggesting increases of $\delta^{34}S$ caused by microbial sulfate

375 reduction. If this is the case, the sulfide-derived sulfate contributions in these sediments would be
376 higher (by up to ~35%). The regional context and interpretation of these sulfur results is discussed
377 somewhat more broadly by Szynkiewicz and Bishop (2021).

378

379 # DISCUSSION

380 ## Chemical and mineralogical stratigraphy

381 Combined spectroscopic, chemical, and mineralogical data from soil pit and core samples suggest
382 distinct trends with depth at the VXE-6 brine pond site (Fig. 15). At 0–4 cm, our results suggest
383 the presence of hydrated salts and/or poorly crystalline aluminosilicates. At 4–6 cm, spectral bands
384 suggest a clay-like material, observation of the highest observed spectral reflectance among all
385 samples analyzed suggests bright material such as clay, elevated Al_2O_3 suggests an
386 aluminosilicate, and elevated major, minor, and trace elemental abundances (including rare earth
387 elements) suggest a chemically active layer. The spectral properties and XRD results of the
388 samples from this horizon are not consistent with montmorillonite or other common Al-rich
389 secondary phyllosilicates, but they are consistent with poorly crystalline aluminosilicates similar
390 to Al-rich phlogopite or mica. At 6–8 cm, spectral and chemical data are consistent with a mixed
391 horizon containing both poorly crystalline aluminosilicates and gypsum. At 8–10 cm, spectral
392 results are highly characteristic of gypsum, and significantly elevated CaO and SO_3 are consistent
393 with the presence of gypsum.

394 ## Aqueous activity and mineral formation in the McMurdo Dry Valleys

The observed assemblages of chlorides, clays, iron oxides/hydroxides, and sulfates indicate a dynamic history of liquid water activity at the VXE-6 pond site in the Wright Valley's South Fork. We suggest that intermittent activity of water within the ephemeral pond and in the shallow subsurface produced the observed mineral assemblages (Fig. 15). Most likely, chemical weathering, freezing, and evaporitic activity (e.g., intermittently present liquid water, changing pond depths and volumes, and attendant changes to solute concentrations/brine composition) drove formation of secondary chlorides and sulfates and aqueous alteration associated with clay formation. Observed chloride salts and gypsum may represent minerals deposited as evaporites at the surface (past and/or present). Alternatively, they could represent minerals accumulated and concentrated at variable depths in the subsurface due to the transient passage of liquid brine of the same origin through the sediments (i.e., shallow groundwater activity) at the pond site. The latter is inferred from negligible variations of $\delta^{34}S$ and $\delta^{18}O$ with depth (Table 6), which suggests a common sulfate ion origin for gypsum. Clays and proto-clays are mainly concentrated at the 4–6 cm depth, suggesting a horizon of elevated aqueous alteration and chemical activity. Precipitation of elemental components from liquid solution during activity of the pond could drive the formation of such clays and explain the notably elevated elemental abundances (e.g., elevated rare earth element abundances due to preferential precipitation from solution; Nesbitt, 1979) at this horizon.

The aqueous and evaporitic processes responsible for formation of the observed mineral assemblages are largely driven by the influence of the hyperarid, cold polar desert conditions prevailing in the McMurdo Dry Valleys. This includes the associated paucity of water stable in liquid form at the surface throughout the region. The relative scarcity of liquid water in the MDV region is controlled by a combination of low precipitation (only as snowfall, without rainfall), high sublimation rates, and subzero °C mean annual air temperatures (Fountain et al., 2010; Obryk et

418 al., 2020). Furthermore, the aqueous activity in the shallow subsurface (and at the surface) is
419 dominated by the impact of permafrost—of an ice table formed due to the subzero °C air
420 temperatures prevailing much of the year, instead of a water table—located at shallow (tens of cm)
421 depths throughout the area (Head and Marchant, 2014). This pervasive, regional permafrost forms
422 an impermeable layer between surface sediments and ephemeral bodies of liquid surface water and
423 underlying deep groundwater systems, and therefore makes mobility of liquid water more difficult
424 (Head and Marchant, 2014). The permafrost aquiclude could, for instance, serve as the lower
425 bound to transient liquid water flow in the shallow sediments at the VXE-6 pond site, with longer-
426 term ponding. Additionally, liquid water may be seasonally present in the sediment immediately
427 overlying the permafrost (e.g., as described by Head and Marchant, 2014), enhancing the aqueous
428 alteration and elemental precipitation responsible for the formation of the observed clay layer. This
429 interstitial liquid water ponded or flowing at the top of the ice table eventually freezes or evaporates
430 (Head and Marchant, 2014). The latter provides a plausible mechanism for the precipitation of
431 salts, gypsum, and any elemental components previously suspended in aqueous solution (e.g., as
432 inferred for the Victoria Valley region by Gibson, 1962). Generally, seasonal melting of sparse
433 snow may provide some transient liquid to the surface and shallow subsurface systems (e.g., as
434 described for parts of the Don Juan basin by Dickson et al., 2013), as may daily or seasonal freeze-
435 thaw cycling in the uppermost ("active") layer of the permafrost (Harris, 1981; Miller and Black,
436 2003).

437

438 ## IMPLICATIONS FOR MARS

439 ### Implications for aqueous activity on Mars

Intermittent aqueous activity and chemical weathering under the cold, xeric conditions prevailing at the VXE-6 pond site in the McMurdo Dry Valleys and the resultant assemblage of chlorides, poorly crystalline aluminosilicates and amorphous material, and gypsum provide a compelling geochemical analog for martian surface processes during the Hesperian period. The Hesperian is interpreted to have been markedly colder and drier than the preceding episodically warm and wet Noachian (namely, too cold for abundant phyllosilicate formation) as evinced by the transition from Noachian Fe/Mg smectites and Al phyllosilicates to poorly crystalline and amorphous phases related to allophane during the later Noachian and early Hesperian age (Bishop and Rampe, 2016; Lowe et al., 2020) to sulfates and chlorides through most of the Hesperian (Ehlmann and Edwards, 2014). For example, investigations of early Hesperian (~3.5 Ga) sedimentary strata during the traverse of the *Curiosity* rover at Gale crater revealed a marked shift from abundant smectites down-section to abundant Ca sulfates moving up-section (Vaniman et al., 2018; Rampe et al., 2020).

Amorphous material. Along the Gale crater transect, X-ray amorphous material has been detected in notable (15–73 wt%) and, as of yet, unexplained abundance (Rampe et al., 2020). A general comparison of these materials to amorphous materials present in modern subglacial sediments at the Three Sisters Volcanic Complex in Oregon suggest subglacial and periglacial weathering (Smith et al. 2018). The occurrence of poorly crystalline and/or amorphous material under largely analogous climatic conditions at the Antarctic VXE-6 pond site may therefore provide important further insight to the development of such amorphous materials in Hesperian-like conditions, and in association with assemblages of cold-weather evaporitic and clay-like minerals. As discussed by Rampe et al. (2020), it should be noted that amorphous materials on Mars must have persisted for up to billions of years without evolving into crystalline phases,

whereas surface sediment in the MDV's Wright Valley was only exposed following Late Quaternary deglaciation, and is generally assumed to be of (younger) glacial origin (McKelvey and Webb, 1962; Calkin et al., 1970; Harris and Cartwright, 1981; Hall et al., 1997).

Chlorides. At Gale crater, chlorides appear infrequently and are inferred to be products of remobilization and reprecipitation, rather than distinctive evaporitic layers within the Murray formation (Thomas et al., 2019). Nonetheless, the surficial salts observed at the VXE-6 pond site are reminiscent of salt crusts observed elsewhere across much of Mars, where lighter colors have long been interpreted as evaporitic deposits (e.g., Clark and Van Hart, 1981). These martian chlorides, observed by the Mars Odyssey Thermal Emission Imaging System in hundreds of localities in southern Mars characterized as irregular depressions (i.e., topographic lows, such as, for instance, a local basin perhaps akin to the VXE-6 basin), have been interpreted as a product of ponding of surface runoff or groundwater upwelling (Osterloo et al., 2010). This is potentially similar in nature to the intermittent activity of water at the VXE-6 pond site, including previous observations of a surface runoff source.

Sulfates. Results from CheMin XRD analyses reveal that gypsum, bassanite, and anhydrite occur frequently at Gale crater (Vaniman et al., 2018). Occasional polyphase associations of these Ca sulfates imply a limited set of equilibrium conditions at the time of formation (Vaniman et al., 2018), thus, identification by XRD of co-occurring gypsum and bassanite (and possible anhydrite) within the Antarctic VXE-6 sediments studied here represents a chance to further constrain geochemical and environmental conditions associated with the formation and co-occurrence of these Ca sulfates, including at Gale crater on Mars.

It is worth noting that beyond Gale crater, Ca sulfate occurrence is widespread on the martian surface (Vaniman et al., 2018). Though anhydrite is not detectable by the spectral methods employed to map mineralogy of the martian surface, gypsum and bassanite have been identified. Expansive gypsum-rich dune fields occur at Olympia Undae (Langevin et al., 2005; Fishbaugh et al., 2007). Gypsum has also been identified at Meridiani Planum (e.g., Grotzinger et al., 2005) and in a trough of Noctis Labyrinthus indicative of Late Hesperian to Amazonian aqueous activity (Weitz et al., 2013. Bassanite has been mainly identified at Mawrth Vallis (Wray et al., 2010).

Clays. Amorphous aluminosilicates are inferred to make up little of the amorphous material identified at Gale crater (Rampe et al., 2020). Therefore, the thin horizon of poorly crystalline aluminosilicates at the VXE-6 pond site, and the ferric oxides/hydroxides produced via chemical weathering of the Ferrar dolerite, could be more analogous in composition (and origin) to poorly crystalline materials identified elsewhere on Mars, including Noctis Labyrinthis (Weitz et al., 2013) and chasma near Valles Marineris (e.g., Weitz et al., 2014).

As discussed above, the proto-clay layer at the VXE-6 site is inferred to have formed via precipitation of elemental components from liquid solution during cold-weather activity of the transient brine pond. This speculated process may provide, by analogy, a mechanism for the formation of amorphous aluminosilicates at ephemeral salt ponds or other sites of transient brine activity in cold, relatively dry environments on ancient Mars. The co-occurrence of aqueous alteration products (salts and clays) with pyroxene at the VXE-6 site may provide clues into the timeline and/or chemistry of this cold-weather alteration mechanism, as demonstrated via the Mars-analog experiments of Phillips-Lander et al. (2019).

Drawing a tentative parallel between the shallow (a few cm to tens of cm) permafrost present in the Antarctica's MDV (Head and Marchant, 2014) and the near-surface (as shallow as a few cm) water ice table on Mars (Piqueux et al., 2019), one might speculate that the martian ice table represents an impermeable layer or aquiclude. Such an aquiclude could be similar to that described in the MDV, thus, the sediment immediately overlying this barrier may be a site of focused water activity whereby any transiently available liquid water (shallow groundwater) is localized. Accordingly, it may be possible that, were liquid water sufficiently available on Mars, development of a chemically altered proto-clay horizon such as that described at the VXE-6 pond site could be possible.

Implications for remote sensing of Mars

As with Mars analog studies at other sites on Earth (e.g., Hawaii's Big Island; Minitti et al., 2007; Yant et al., 2018; Calvin et al., 2020; California's Mojave Desert; Peters et al., 2008; Bonaccorsi et al., 2020; Spain's Canary Islands; Burton et al., 2020; Wyoming's Yellowstone National Park; Hinman et al., 2021), as well as previous analog studies in Antarctica (e.g., Gibson et al., 1983), the chemical and mineralogical results reported here for the VXE-6 pond site have implications for remote sensing applications on the martian surface. Changing spectral features that are seen with changing depths at the VXE-6 pond site could be applied to remote sensing data received from Mars. In particular, spectral patterns noted here could aid in identifying evidence of ancient salt ponds on the martian surface. These patterns could be applied in deconvolving spectral signals in regions with fine-scale associations of mineralogies, such as the thin outcrops of varying sulfates, opal, and poorly crystalline materials identified at sites such as Noctis Labyrinthus and Coprates Chasma (e.g., Weitz et al., 2013).

527

528 ## ACKNOWLEDGEMENTS AND FUNDING

529 Z.F.M.B. thanks the Clay Minerals Society (CMS Travel Award and CMS Research Grant) and
530 the Geological Society of America (GSA Graduate Student Research Grant) for funding. Z.F.M.B.
531 and J.L.B. thank the NASA Astrobiology Institute (NAI #NNX15BB01) for support. We thank
532 Takahiro Hiroi at Brown University for assistance with RELAB spectral measurements, Shital
533 Patel for assistance with spectral data processing, Dieter Mader for help with INAA data
534 collection, and Henry Harris for insightful discussions of the VXE-6 site and surrounding region.
535 This manuscript benefited from the comments and suggestions of two anonymous reviewers.

536

537 ## REFERENCES CITED

538 Allen C. C. and Conca J. L. (1991) Weathering of basaltic rocks under cold, arid conditions:
539 Antarctica and Mars. Proc. Lunar Planet. Sci. Conf. 21, 711-717.

540 Anderson D. M., Gatto L. W. and Ugolini F. C. (1972) An Antarctic analog of martian permafrost
541 terrain. Antarctic Journal of the United States 7, 114-116.

542 Ansan V., Mangold N., Masson P., Gailhardis E. and Neukum G. (2008) Topography of valley
543 networks on Mars from Mars Express High Resolution Stereo Camera digital elevation
544 models. Journal of Geophysical Research 113, doi:10.1029/2007JE002986.

545 Bandfield J. L. (2002) Global mineral distributions on Mars. Journal of Geophysical Research:
546 Planets 107, doi:10.1029/2001JE001510.

Bao H. and Marchant D. R. (2006) Quantifying sulfate components and their variations in soils of the McMurdo Dry Valleys, Antarctica. Journal of Geophysical Research: Atmospheres 111, doi:10.1029/2005JD006669.

Barrett P. J., Elliot D. H. and Lindsay J. F. (1986) The Beacon Supergroup (Devonian-Triassic) and Ferrar Group (Jurrasic) in the Beardmore Glacier Area, Antarctica. Antarctic Research Series 36, 339-428.

Bédard J. H., Marsh B. D., Hersum T. G., Naslund H. R. and Mukasa S. B. (2007) Large-scale mechanical redistribution of orthopyroxene and plagioclase in the Basement Sill, Ferrar Dolerites, McMurdo Dry Valleys, Antarctica: petrological, mineral-chemical and field evidence for channelized movement of crystals and melt. Journal of Petrology 48, 2289-2326.

Bibring J. P., Langevin Y., Gendrin A., Gondet B., Poulet F., Berthé M., Soufflot A., Arvidson R., Mangold N., Mustard J. F. and Drossart P. (2005) Mars surface diversity as revealed by the OMEGA/Mars Express observations. Science 307, 1576-1581.

Bibring J. P., Langevin Y., Mustard J. F., Poulet F., Arvidson R., Gendrin A., et al. (2006) Global mineralogical and aqueous Mars history derived from OMEGA/Mars Express data. Science 312, 400-404.

Bishop J. L. (2018) Chapter 3: Remote detection of phyllosilicates on Mars and implications for climate and habitability. In From Habitability to Life on Mars (eds. N. A. Cabrol and E. A. Grin). Elsevier. pp. 37-75.

567 Bishop J. L. and Rampe E. B. (2016) Evidence for a changing martian climate from the mineralogy
568 at Mawrth Vallis. Earth and Planetary Science Letters 448, 42-48.

569 Bishop J. L., Koeberl C., Kralik C., Fröschl H., Enolert P. A., Andersen D. W., Pieters C. M. and
570 Wharton, Jr, R. A. (1996) Reflectance spectroscopy and geochemical analyses of Lake
571 Hoare sediments, Antarctica: Implications for remote sensing of the Earth and Mars.
572 Geochimica et Cosmochimica Acta 60, 765-785.

573 Bishop J. L., Lougear A., Newton J., Doran P. T., Froeschl H., Trautwein A. X., Körner W. and
574 Koeberl C. (2001) Mineralogical and geochemical analyses of Antarctic lake sediments: a
575 study of reflectance and Mössbauer spectroscopy and C, N, and S isotopes with
576 applications for remote sensing on Mars. Geochimica et Cosmochimica Acta 65, 2875-
577 2897.

578 Bishop J. L., Anglen B. L., Pratt L. M., Edwards H. G., Des Marais D. J. and Doran P. T. (2003)
579 A spectroscopy and isotope study of sediments from the Antarctic Dry Valleys as
580 analogues for potential paleolakes on Mars. International Journal of Astrobiology 2, 273.

581 Bishop J. L., Dobrea E. Z. N., McKeown N. K., Parente M., Ehlmann B. L., Michalski J. R., et al.
582 (2008) Phyllosilicate diversity and past aqueous activity revealed at Mawrth Vallis, Mars.
583 Science 321, 830-833.

584 Bishop J. L., Rampe E. B., Bish D. L., Baker L. L., Abidin Z., Matsue N. and Henmi T. (2013)
585 Spectral and hydration properties of allophane and imogolite. Clays and Clay Minerals 61,
586 57-74.

587 Bishop J. L., Englert P. A., Patel S., Tirsch D., Roy A. J., Koeberl C., Böttger U., Hanke F. and
588 Jaumann R. (2014a) Mineralogical analyses of surface sediments in the Antarctic Dry
589 Valleys: coordinated analyses of Raman spectra, reflectance spectra and elemental
590 abundances. Philosophical Transactions of the Royal Society A: Mathematical, Physical
591 and Engineering Sciences 372, doi:10.1098/rsta.2014.0198.

592 Bishop J. L., Lane M. D., Dyar M. D., King S. J., Brown A. J. and Swayze G. A. (2014b) Spectral
593 properties of Ca-sulfates: Gypsum, bassanite, and anhydrite. American Mineralogist 99,
594 2105-2115.

595 Bishop J. L., Fairén A. G., Michalski J. R., Gago-Duport L., Baker L. L., Velbel M. A., Gross C.
596 and Rampe E. B. (2018) Surface clay formation during short-term warmer and wetter
597 conditions on a largely cold ancient Mars. Nature Astronomy 2, 206-213.

598 Bishop J. L., Yeşilbaş M., Hinman N. W., Burton Z. F. M., Englert P. A. J., Toner J. D., McEwen
599 A. S., Gulick V. C., Gibson E. K. and Koeberl C. (2021) Martian subsurface cryosalt
600 expansion and collapse as trigger for landslides. Science Advances 7, eabe4459,
601 doi:10.1126/sciadv.abe4459.

602 Blake D. F., Morris R. V., Kocurek G., Morrison S. M., Downs R. T., Bish D. et al. (2013)
603 Curiosity at Gale crater, Mars: Characterization and analysis of the Rocknest sand shadow.
604 Science 341, doi:10.1126/science.1239505.

605 Bockheim J. G. (2002) Landform and soil development in the McMurdo Dry Valleys, Antarctica:
606 a regional synthesis. Arctic, Antarctic, and Alpine Research 34, 308-317.

607 Burton Z. F. M., Bishop J. L. and Danielsen J. M. (2020) Altered volcanic material from
608 Fuerteventura, Spain as a possible analogue for the martian surface. 51st Lunar and
609 Planetary Science Conference. The Woodlands, TX. Abstract #1713.

610 Bristow T. F., Rampe E. B., Achilles C. N., Blake D. F., Chipera S. J., Craig P. et al. (2018). Clay
611 mineral diversity and abundance in sedimentary rocks of Gale crater, Mars. Science
612 Advances 4, doi:10.1126/sciadv.aar3330.

613 Bristow T. F., Grotzinger J. P., Rampe E. B., Cuadros J., Chipera S. J., Downs G. W. et al. (2021)
614 Brine-driven destruction of clay minerals in Gale crater, Mars. Science 373, 198-204.

615 Bull C. (1965) Climatological Observations in Ice-Free Areas of Southern Victoria Land,
616 Antarctica. Antarctic Research Series 9, 177-194.

617 Bonaccorsi R., Bishop J. L. and Burton Z. F. M. (2020) Salty clay sites in the Mojave Desert as
618 analogues for Mars: VNIR spectroscopy investigations of fluvio-lacustrine volcaniclastic
619 deposits. 51st Lunar and Planetary Science Conference. The Woodlands, TX. Abstract
620 #2525.

621 Calkin P. E., Behling R. E. and Bull C. (1970) Glacial history of Wright Valley, southern Victoria
622 Land, Antarctica. Antarctic Journal of the United States 5, 22-27.

623 Calvin W. M., Lautze N., Moore J., Thomas D., Haskins E. and Rasmussen B. P. (2020)
624 Petrographic and spectral study of hydrothermal mineralization in drill core from Hawaii:
625 A potential analog to alteration in the martian subsurface. American Mineralogist 105,
626 1297-1305.

627 Campbell I. B. and Claridge G. G. C. (1982) The influence of moisture on the development of soils
628 of the cold deserts of Antarctica. Geoderma 28, 221-238.

629 Carr M. H. (1987) Water on Mars. Nature 326, 30-35.

630 Carr M. H. (1996) Water on Mars. Oxford University Press, Oxford.

631 Carter J., Loizeau D., Mangold N., Poulet F. and Bibring J. P. (2015) Widespread surface
632 weathering on early Mars: A case for a warmer and wetter climate. Icarus 248, 373-382.

633 Christensen P. R., Bandfield J. L., Hamilton V. E., Ruff S. W., Kieffer H. H., Titus T. N. et al.
634 (2001) Mars Global Surveyor Thermal Emission Spectrometer experiment: investigation
635 description and surface science results. Journal of Geophysical Research: Planets 106,
636 doi:10.1029/2000JE001370.

637 Claridge G. G. C. (1965) The clay mineralogy and chemistry of some soils from the Ross
638 Dependency, Antarctica. New Zealand Journal of Geology and Geophysics 8, 186-220.

639 Claridge G. G. C. and Campbell I. B. (1977) The salts in Antarctic soils, their distribution and
640 relationship to soil processes. Soil Science 123, 377-384.

641 Claridge G. G. C. and Campbell I. B. (1984) Mineral transformation during the weathering of
642 dolerite under cold arid conditions in Antarctica. New Zealand Journal of Geology and
643 Geophysics 27, 537-545.

644 Clark B. C. and Van Hart D. C. (1981) The salts of Mars. Icarus 45, 370-378.

645 Clark B. C. (1993) Geochemical components in Martian soil. Geochimica et Cosmochimica Acta
646 57, 4575-4581.

Clarkson P. D. (1981) Geology of the Shackleton Range: IV. The dolerite dykes. British Antarctic Survey Bulletin 53, 201-212.

Craddock R. A. and Howard A. D. (2002) The case for rainfall on a warm, wet early Mars. Journal of Geophysical Research: Planets 107, doi:10.1029/2001JE001505.

Dickson J. L., Head J. W., Levy J. S. and Marchant D. R. (2013) Don Juan Pond, Antarctica: Near-surface CaCl 2-brine feeding Earth's most saline lake and implications for Mars. Scientific Reports 3, doi:10.1038/srep01166.

Ehlmann, B.L., Mustard J.F., Swayze G.A., Clark R.N., Bishop J.L., Poulet F., Marais D.J.D., Roach L.H., Milliken R.E., Wray J.J., Barnouin-Jha O., and Murchie S.L. (2009) Identification of hydrated silicate minerals on Mars using MRO-CRISM: Geologic context near Nili Fossae and implications for aqueous alteration. Journal of Geophysical Research, 114, doi:10.1029/2009JE003339.Ehlmann B. L. and Edwards C. S. (2014) Mineralogy of the Martian Surface. Annual Review of Earth and Planetary Sciences 42, 291-315.

Elliot D. H., Fleck R. J. and Sutter J. F. (1985) Potassium-argon age determinations of Ferrar Group rocks, central Transantarctic Mountains. In Geology of the Central Transantarctic Mountains, Antarctic Research Series, Vol. 36 (eds. M. D. Turner and J. F. Splettstoesser). American Geophysical Union, Washington, D.C. pp. 197-224.

Fassett C. I. and Head III, J. W. (2008a) The timing of Martian valley network activity: Constraints from buffered crater counting. Icarus 195, 61-89.

Fassett C. I. and Head III, J. W. (2008b) Valley network-fed, open-basin lakes on Mars: Distribution and implications for Noachian surface and subsurface hydrology. Icarus 198, 37-56.

Fassett C. I. and Head III, J. W. (2011) Sequence and timing of conditions on early Mars. Icarus 211, 1204-1214.

Fishbaugh K. E., Poulet F., Chevrier V., Langevin Y. and Bibring J. P. (2007) On the origin of gypsum in the Mars north polar region. Journal of Geophysical Research: Planets 112, doi:10.1029/2006JE002862.

Fountain A. G., Nylen T. H., Monaghan A., Basagic H. J. and Bromwich D. (2010) Snow in the McMurdo Dry Valleys, Antarctica. International Journal of Climatology: A Journal of the Royal Meteorological Society 30, 633-642.

Gellert R. and Yen A. S. (2019) Chapter 28: Elemental Analyses of Mars from Rovers Using the Alpha-Particle X-Ray Spectrometer. In Remote Compositional Analysis: Techniques for Understanding Spectroscopy, Mineralogy, and Geochemistry of Planetary Surfaces (eds. J. L. Bishop, J. F. Bell III and J. E. Moersch). Cambridge University Press, Cambridge, UK. pp. 555-572.

Gibson G. W. (1962) Geological Investigations in Southern Victoria Land, Antarctica: Part 8—Evaporite salts in the Victoria Valley Region. New Zealand Journal of Geology and Geophysics 5, 361-374.

685 Gibson E. K., Wentworth S. J. and McKay D. S. (1983) Chemical weathering and diagenesis of a
686 cold desert soil from Wright Valley, Antarctica: An analog of Martian weathering
687 processes. Journal of Geophysical Research: Solid Earth 88, A912-A928.

688 Glotch T. D., Bandfield J. L., Tornabene L. L., Jensen H. B. and Seelos F. P. (2010) Distribution
689 and formation of chlorides and phyllosilicates in Terra Sirenum, Mars. Geophysical
690 Research Letters 37, doi:10.1029/2010GL044557.

691 Gough R. V., Chevrier V. F. and Tolbert M. A. (2016) Formation of liquid water at low
692 temperatures via the deliquescence of calcium chloride: Implications for Antarctica and
693 Mars. Planetary and Space Science 131, 79-87.

694 Greeley R. and Spudis, P. D. (1981) Volcanism on Mars. Reviews of Geophysics 19, 13-41.

695 Grotzinger J. P., Arvidson R. E., Bell III, J. F., Calvin W., Clark B. C., Fike D. A. et al. (2005)
696 Stratigraphy and sedimentology of a dry to wet eolian depositional system, Burns
697 formation, Meridiani Planum, Mars. Earth and Planetary Science Letters 240, 11-72.

698 Haberle R. M., McKay C. P., Schaeffer J., Cabrol N. A., Grin E. A., Zent A. P. and Quinn R.
699 (2001) On the possibility of liquid water on present-day Mars. Journal of Geophysical
700 Research: Planets 106, 23317-23326.

701 Hagen E. H. (1988) Geochemical studies of Neogene till in the Transantarctic Mountains:
702 Evidence for an extraterrestrial component. M.S. thesis, The Ohio State University.

703 Hall B. L., Denton G. H., Lux D. R. and Schlüchter C. (1997) Pliocene paleoenvironment and
704 Antarctic ice sheet behavior: evidence from Wright Valley. The Journal of Geology 105,
705 285-294.

706 Harrington H. J. (1958) Nomenclature of rock units in the Ross Sea region, Antarctica. Nature
707 182, 290-290.

708 Harris H. J. H. (1981) Hydrology and hydrogeochemistry of the South Fork, Wright Valley,
709 Southern Victoria Land, Antarctica. Ph.D. thesis, Univ. of Illinois, Urbana.

710 Harris H. J. H. and Cartwright K. (1981) Hydrology of the Don Juan Basin, Wright Valley,
711 Antarctica. Antarctic Research Series 33, 161-184.

712 Hartmann W. K., Malin M., McEwen A., Carr M., Soderblom L., Thomas P., Danielson E., James
713 P. and Veverka J. (1999) Evidence for recent volcanism on Mars from crater counts. Nature
714 397, 586-589.

715 Harvey R. P. (2001) The Ferrar Dolerite: An Antarctic analog for martian basaltic lithologies and
716 weathering processes. In Field Trip and Workshop on the Martian Highlands and Mojave
717 Desert Analogs. Abstract #4012.

718 Hauber E., Brož P., Jagert F., Jodłowski P. and Platz T. (2011) Very recent and wide-spread
719 basaltic volcanism on Mars. Geophysical Research Letters 38,
720 doi:10.1029/2011GL047310.

721 Head J. W. and Marchant D. R. (2014) The climate history of early Mars: insights from the
722 Antarctic McMurdo Dry Valleys hydrologic system. Antarctic Science 26, 774-800.

723 Hinman N. W., Bishop J. L., Gulick V. C., Dettmann J. M. K., Morkner P., Berlanga G.,
724 Henneberger R. M., Bergquist P., Richardson C. D., Walter M. R. and MacKenzie L. A.
725 (2021) Targeting mixtures of jarosite and clay minerals for Mars exploration. American
726 Mineralogist: Journal of Earth and Planetary Materials 106, 1237-1254.

727 Hynek B. M., Osterloo M. K. and Kierein-Young K. S. (2015) Late-stage formation of Martian
728 chloride salts through ponding and evaporation. Geology 43, 787-790.

729 King S. J., Bishop J. L., Fenton L. K., Lafuente B., Garcia G. C. and Horgan B. H. (2013) VNIR
730 reflectance spectra of gypsum mixtures for comparison with White Sands National
731 Monument, New Mexico (WSNM) dune samples as an analog study of the Olympia Undae
732 region of Mars. American Geophysical Union Fall Meeting. San Francisco, CA. Abstract
733 #P23C-1800.

734 Kite E. S. (2019) Geologic constraints on early Mars climate. Space Science Reviews 215,
735 doi:10.1007/s11214-018-0575-5.

736 Koeberl C. (1993) Instrumental neutron activation analysis of geochemical and cosmochemical
737 samples: a fast and reliable method for small sample analysis. Journal of Radioanalytical
738 and Nuclear Chemistry 168, 47-60.

739 Langevin Y., Poulet F., Bibring J. P. and Gondet B. (2005) Sulfates in the north polar region of
740 Mars detected by OMEGA/Mars Express. Science 307, 1584-1586.

741 Lauro F. M., DeMaere M. Z., Yau S., Brown M. V., Ng C., Wilkins D. et al. (2011) An integrative
742 study of a meromictic lake ecosystem in Antarctica. The ISME Journal 5, 879-895.

743 Lowe D. R., Bishop J. L., Loizeau D., Wray J. J. and Beyer R. A. (2020) Deposition of >3.7 Ga
744 clay-rich strata of the Mawrth Vallis Group, Mars, in lacustrine, alluvial, and aeolian
745 environments. GSA Bulletin 132, 17-30.

746 Mader D. and Koeberl C. (2009) Using Instrumental Neutron Activation Analysis for geochemical
747 analyses of terrestrial impact structures: Current analytical procedures at the University of

748 Vienna Geochemistry Activation Analysis Laboratory. Applied Radiation and Isotopes 67,
749 2100-2103.

750 Mancinelli R. L. (2004) Microbial Life in Brines, Evaporites and Saline Sediments: The Search
751 for Life on Mars. In Water on Mars and Life. Springer, Berlin, Heidelberg. pp. 277-297.

752 Mayer B. and Krouse H. R. (2004) Procedures for sulfur isotope abundance studies. In Handbook
753 of Stable Isotope Analytical Techniques (ed. P. A. De Groot). Elsevier, Amsterdam. pp.
754 538-596.

755 McCraw J. D. (1967) Soils of Taylor Dry Valley, Victoria Land, Antarctica, with notes on soils
756 from other localities in Victoria Land. New Zealand Journal of Geology and Geophysics
757 10, 498-539.

758 McDonough W. F. and Sun S. S. (1995) The composition of the Earth. Chemical Geology 120,
759 223-253.

760 McKelvey B. C. and Webb P. N. (1962) Geological investigations in Southern Victoria Land,
761 Antarctica: Part 3—Geology of Wright Valley. New Zealand Journal of Geology and
762 Geophysics 5, 143-162.

763 McLennan S. M., Anderson R. B., Bell J. F., Bridges J. C., Calef F., Campbell J. L. et al. (2014)
764 Elemental geochemistry of sedimentary rocks at Yellowknife Bay, Gale crater, Mars.
765 Science 343, doi:10.1126/science.1244734.

766 McLeod M., Bockheim J., Balks M. R. and Aislabie J. M. (2009) Soils of western Wright Valley,
767 Antarctica. Antarctic Science 21, 355–365

McSween, Jr., H. Y. (2002) The rocks of Mars, from far and near. Meteoritics & Planetary Science 37, 7-25.

Mikucki J. A., Pearson A., Johnston D. T., Turchyn A. V., Farquha, J., Schrag D. P. et al. (2009) A contemporary microbially maintained subglacial ferrous "ocean." Science 324, 397-400.

Miller R. D. and Black P. B. (2003) Redistribution of water in terrestrial soils at subfreezing temperatures: A review of processes and their potential relevance to Mars. Journal of Geophysical Research: Planets 108, doi:10.1029/2002JE001873.

Minitti M. E., Weitz C. M., Lane M. D. and Bishop J. L. (2007) Morphology, chemistry, and spectral properties of Hawaiian rock coatings and implications for Mars. Journal of Geophysical Research: Planets 112, doi:10.1029/2006JE002839.

Morris E. C., Holt H. E., Mutch T. A. and Lindsay J. F. (1972) Mars analog studies in Wright and Victoria Valleys, Antarctica. Antarctic Journal of the United States 7, 113-114.

Murchie S. L., Mustard J. F., Ehlmann B. L., Milliken R. E., Bishop J. L., McKeown N. K. and Bibring J. P. (2009) A synthesis of Martian aqueous mineralogy after 1 Mars year of observations from the Mars Reconnaissance Orbiter. Journal of Geophysical Research: Planets 114, doi:10.1029/2009JE003342.

Murchie S. L., Bibring J. P., Arvidson R. E., Bishop J. L., Carter J., Ehlmann B. L., Langevin Y., Mustard J. F., Poulet F., Riu L., Seelos K. D. and Viviano C. E. (2019) Chapter 23. Visible to short-wave Infrared spectral analyses of Mars from orbit using CRISM and OMEGA. In Remote Compositional Analysis: Techniques for Understanding Spectroscopy,

Mineralogy, and Geochemistry of Planetary Surfaces (eds. J. L. Bishop, J. E. Moersch and J. F. Bell III). Cambridge University Press, Cambridge, UK. pp. 453-483.

Murray A. E., Kenig F., Fritsen C. H., McKay C. P., Cawley K. M., Edwards R. et al. (2012) Microbial life at −13 °C in the brine of an ice-sealed Antarctic lake. Proceedings of the National Academy of Sciences 109, 20626-20631.

Mustard J. F., Murchie S. L., Pelkey S. M., Ehlmann B. L., Milliken R. E., Grant J. A. et al. (2008) Hydrated silicate minerals on Mars observed by the Mars Reconnaissance Orbiter CRISM instrument. Nature 454, 305-309.

Nedell S. S., Andersen D. W., Squyres S. W. and Love F. G. (1987) Sedimentation in ice-covered Lake Hoare, Antarctica. Sedimentology 34, 1093-1106.

Nesbitt H. W. (1979) Mobility and fractionation of rare earth elements during weathering of a granodiorite. Nature 279, 206-210.

Obryk M. K., Doran P. T., Fountain A. G., Myers M. and McKay C. P. (2020) Climate from the McMurdo Dry Valleys, Antarctica, 1986–2017: Surface air temperature trends and redefined summer season. Journal of Geophysical Research: Atmospheres 125, doi:10.1029/2019JD032180.

Osterloo M. M., Hamilton V. E., Bandfield J. L., Glotch T. D., Baldridge A. M., Christensen P. R. et al. (2008). Chloride-bearing materials in the southern highlands of Mars. Science 319, 1651-1654.

Osterloo M. M., Anderson F. S., Hamilton V. E. and Hynek B. M. (2010) Geologic context of proposed chloride-bearing materials on Mars. Journal of Geophysical Research: Planets 115, doi:10.1029/2010JE003613.

Peters G. H., Abbey W., Bearman G. H., Mungas G. S., Smith J. A., Anderson R. C. et al. (2008) Mojave Mars simulant—Characterization of a new geologic Mars analog. Icarus 197, 470-479.

Phillips-Lander C. M., Madden A. S. E., Hausrath E. M. and Madden M. E. E. (2019) Aqueous alteration of pyroxene in sulfate, chloride, and perchlorate brines: Implications for post-Noachian aqueous alteration on Mars. Geochimica et Cosmochimica Acta 257, 336-353.

Piqueux S., Buz J., Edwards C. S., Bandfield J. L., Kleinböhl A., Kass D. M. et al. (2019) Widespread shallow water ice on Mars at high latitudes and midlatitudes. Geophysical Research Letters 46, 14290-14298.

Poulet F., Bibring J. P., Mustard J. F., Gendrin A., Mangold N., Langevin Y. et al. (2005) Phyllosilicates on Mars and implications for early Martian climate. Nature 438, 623-627.

Rampe E. B., Kraft M. D., Sharp T. G., Golden D. C., Ming D. W. and Christensen P. R. (2012) Allophane detection on Mars with Thermal Emission Spectrometer data and implications for regional-scale chemical weathering processes. Geology 40, 995-998.

Rampe E. B., Blake D. F., Bristow T. F., Ming D. W., Vaniman D. T., Morris R. V. et al. (2020) Mineralogy and geochemistry of sedimentary rocks and eolian sediments in Gale crater, Mars: A review after six Earth years of exploration with Curiosity. Geochemistry 80, doi:10.1016/j.chemer.2020.125605.

828 Samarkin V. A., Madigan M. T., Bowles M. W., Casciotti K. L., Priscu J. C., McKay C. P. and
829 Joye S. B. (2010) Abiotic nitrous oxide emission from the hypersaline Don Juan Pond in
830 Antarctica. Nature Geoscience 3, 341-344.

831 Shaw S. E. (1962) Petrography of Beacon sandstone samples from Beacon Height West, upper
832 Taylor Glacier, Antarctica. New Zealand Journal of Geology and Geophysics 5, 733-739.

833 Small H., Stevens T. S. and Bauman W. C. (1975) Novel ion exchange chromatographic method
834 using conductimetric detection. Analytical Chemistry 47, 1801-1809.

835 Smith R. J., Rampe E. B., Horgan B. H. and Dehouck E. (2018) Deriving amorphous component
836 abundance and composition of rocks and sediments on Earth and Mars. Journal of
837 Geophysical Research: Planets 123, 2485-2505.

838 Squyres S. W., Grotzinger J. P., Arvidson R. E., Bell J. F., Calvin W., Christensen P. R. and
839 Soderblom L. A. (2004) In situ evidence for an ancient aqueous environment at Meridiani
840 Planum, Mars. Science 306, 1709-1714.

841 Sun T., Socki R. A., Bish D. L., Harvey R. P., Bao H., Niles P. B. et al. (2015) Lost cold Antarctic
842 deserts inferred from unusual sulfate formation and isotope signatures. Nature
843 Communications 6, 1-7.

844 Szynkiewicz A. and Bishop J. L. (2021) Assessment of Sulfate Sources under Cold Conditions as
845 a Geochemical Proxy for the Origin of Sulfates in the Circumpolar Dunes on Mars.
846 Minerals 11, doi:10.3390/min11050507.

847 Szynkiewicz A., Bishop J. L. and Burton Z. F. M. (2021) Review of Sulfate Sources in Antarctic
848 Polar Environments—Geochemical Implications for Sulfate Origin on Mars. 52nd Lunar
849 and Planetary Science Conference. Abstract #1366.

850 Thomas N. H., Ehlmann B. L., Meslin P. Y., Rapin W., Anderson D. E., Rivera-Hernández F. et
851 al. (2019) Mars Science Laboratory observations of chloride salts in Gale crater, Mars.
852 Geophysical Research Letters 46, 10754-10763.

853 Thompson D. C., Bromley A. M. and Craig R. M. F. (1971) Ground temperatures in an Antarctic
854 dry valley. New Zealand Journal of Geology and Geophysics 14, 477-483.

855 Toner J. D., Sletten R. S. and Prentice M. L. (2013) Soluble salt accumulations in Taylor Valley,
856 Antarctica: implications for paleolakes and Ross Sea Ice Sheet dynamics. Journal of
857 Geophysical Research: Earth Surface 118, 198-215.

858 Tosca N. J. and Knoll A. H. (2009) Juvenile chemical sediments and the long term persistence of
859 water at the surface of Mars. Earth and Planetary Science Letters 286, 379-386.

860 Ugolini F. C. and Anderson D. M. (1973) Ionic migration and weathering in frozen Antarctic soils.
861 Soil Science 115, 461-470.

862 Vaniman D. T., Bish D. L., Ming D. W., Bristow T. F., Morris R. V., Blake D. F. et al. (2014)
863 Mineralogy of a mudstone at Yellowknife Bay, Gale crater, Mars. Science 343,
864 doi:10.1126/science.1243480.

865 Vaniman D. T., Martínez G. M., Rampe E. B., Bristow T. F., Blake D. F., Yen A. S. et al. (2018)
866 Gypsum, bassanite, and anhydrite at Gale crater, Mars. American Mineralogist 103, 1011-
867 1020.

Velbel M. A. (2012) Aqueous alteration in Martian meteorites: Comparing mineral relations in igneous-rock weathering of Martian meteorites and in the sedimentary cycle of Mars. In Sedimentary Geology of Mars (eds. J. P. Grotzinger and R. E. Milliken). SEPM Special Publication 102, 97-112.

Warner N., Gupta S., Lin S. Y., Kim J. R., Muller J. P. and Morley J. (2010) Late Noachian to Hesperian climate change on Mars: Evidence of episodic warming from transient crater lakes near Ares Vallis. Journal of Geophysical Research: Planets 115, doi:10.1029/2009JE003522.

Weitz C. M., Bishop J. L. and Grant J. A. (2013) Gypsum, opal, and fluvial channels within a trough of Noctis Labyrinthus, Mars: Implications for aqueous activity during the Late Hesperian to Amazonian. Planetary and Space Science 87, 130-145.

Weitz C. M., Bishop J. L., Baker L. L. and Berman D. C. (2014) Fresh exposures of hydrous Fe-bearing amorphous silicates on Mars. Geophysical Research Letters 41, 8744-8751.

Wentworth S. J., Gibson E. K., Velbel M. A. and McKay D. S. (2005) Antarctic Dry Valleys and indigenous weathering in Mars meteorites: Implications for water and life on Mars. Icarus 174, 383-395.

Wilson L. and Head III, J. W. (1994) Mars: Review and analysis of volcanic eruption theory and relationships to observed landforms. Reviews of Geophysics 32, 221-263.

Wordsworth R. D. (2016) The climate of early Mars. Annual Review of Earth and Planetary Sciences 44, 381-408.

888 Wray J. J., Squyres S. W., Roach L. H., Bishop J. L., Mustard J. F. and Dobrea E. Z. N. (2010)
889 Identification of the Ca-sulfate bassanite in Mawrth Vallis, Mars. Icarus 209, 416-421.

890 Yant M., Young K. E., Rogers A. D., McAdam A. C., Bleacher J. E., Bishop J. L. and Mertzman,
891 S. A. (2018) Visible, near-infrared, and mid-infrared spectral characterization of Hawaiian
892 fumarolic alteration near Kilauea's December 1974 flow: Implications for spectral
893 discrimination of alteration environments on Mars. American Mineralogist: Journal of
894 Earth and Planetary Materials 103, 11-25.

FIGURE 1. (a) Study area in Wright Valley's South Fork; white box indicates the VXE-6 pond site and sampling sites discussed herein; red box on inset map of Antarctica indicates general location of Wright Valley; DJP—Don Juan Pond, MDV—McMurdo Dry Valleys. Photo credit: NASA EO-1, 2014. (b) Representative photograph of the area surrounding the VXE-6 pond. Photo credit: Everett K. Gibson, NASA-JSC, 1980. (c) Photograph of the VXE-6 pond site (facing ~West) from which soil pit and core samples were collected in 1980. Photo credit: Everett K. Gibson, NASA-JSC, 1980.

FIGURE 2. (a) Soil pit samples in original form as collected in 1980; 5 cm scale applies to all panels. (b) Finely crushed soil pit sample aliquots prepared in 1983; 3 cm scale applies to all panels. Note that apparent differences in brightness between (a) and (b) at identical sample depths are primarily due to differences in lighting and, to some degree, moisture content. (c) Photograph of core collected in 1980.

FIGURE 3. Mineral abundances determined by XRD of soil pit samples from the VXE-6 pond site. Note that minerals are split between the top and bottom panels solely to aid in visualization of the data.

FIGURE 4. Example of the XRD diffraction patterns obtained for the VXE-6 pond site soil pit samples (black line indicates experimental data, red line indicates model fit). This diffraction

915 pattern for sample JB1103 illustrates the elevated abundance of gypsum at the 8–10 cm depth
916 interval.

917

918 **FIGURE 5.** VNIR reflectance spectra of the six soil pit samples from the VXE-6 pond site
919 compared to spectra of montmorillonite, allophane, gypsum, anhydrite, and halite. Mineral spectra
920 are from previous work of Bishop and coauthors (e.g., Bishop et al., 2008, 2013, 2014b).

921

922 **FIGURE 6.** VNIR reflectance spectra of the ten core samples from the VXE-6 pond site. Spectra
923 of the samples from 8–10 cm are consistent with gypsum, while the upper sediments contain other
924 hydrated phases.

925

926 **FIGURE 7.** Mid-IR reflectance spectra. (a) Spectra of the ten core samples from the VXE-6 pond
927 site. (b) Spectra of the deeper core samples compared with spectra of quartz, a quartz/gypsum
928 mixture, gypsum, and bassanite. Quartz bands are marked by dashed grey lines, while gypsum and
929 bassanite bands are marked by pink and purple vertical lines. Spectra of these minerals and
930 mixtures are from King et al. (2013) and Bishop et al. (2014b).

931

932 **FIGURE 8.** Normalized H_2O band depths near 1.92 μm for the VXE-6 soil pit samples.

933

934 **FIGURE 9.** VNIR spectra of four different sample preparations for two soil pit samples: FA
935 (finely-crushed particles prepared in 1983; Gibson et al., 1983), GA (ground, <125 μm fractions
936 prepared in 2018), and CA (coarse original sediment grains) were measured under ambient
937 conditions using the ASD spectrometer at the SETI Institute, while FD (finely-crushed particles
938 prepared in 1983) was measured under controlled dry conditions at RELAB. (a) 0–1 sample depth.
939 (b) 8–10 cm sample depth.

940

941 **FIGURE 10.** VNIR spectra of finely-crushed VXE-6 soil pit samples measured at RELAB under
942 dry controlled (brown lines) and ambient (blue lines) conditions.

943

944 **FIGURE 11.** Elemental abundances from INAA for the VXE-6 soil pit samples; *denotes
945 abundance in wt% rather than ppm.

946

947 **FIGURE 12.** Chondrite-normalized (using normalization values of McDonough and Sun, 1995)
948 rare earth element abundances for all soil pit samples from the VXE-6 pond site.

949

950 **FIGURE 13.** XRF major element abundances by depth for soil pit samples from the VXE-6 pond
951 site.

952

953 **FIGURE 14.** Comparison of $\delta^{34}S$ and $\delta^{18}O$ of sulfates from VXE-6 soil pit (this study) and other
954 areas of Antarctica (Bao and Marchant, 2006; Mikucki et al., 2009; Lauro et al., 2011; Sun et al.,
955 2015). Mixing line is determined for the sulfide- and seawater-derived sulfate inputs into the soils
956 of MDV. The $\delta^{34}S$ of sulfide-derived sulfate is based on SSE results (this study) and $\delta^{18}O$ is based
957 on the isotope composition of surface water and groundwater (Harris, 1981; Mikucki et al., 2009;
958 Sun et al., 2015).

959

960 **FIGURE 15.** Schematic summary of the observed aqueous mineral assemblage at the VXE-6
961 pond site and of the aqueous processes interpreted to be responsible for the formation of these
962 chemical and mineralogical trends.

963

Soil pit samples		*Core samples*	
Sample ID	**Sample depth (cm)**	**Sample ID**	**Sample depth (cm)**
JB1100	0–1	JB1303	0–1
JB1101	1–4	JB1304	1–2
		JB1305	2–3
		JB1306	3–4
JB1102	4–7	JB1307	4–5
		JB1308	5–6
		JB1309	6–7
		JB1310	7–8
JB1103	8–10	JB1311	8–9
		JB1312	9–10
		JB1313	10–11
		JB1314	11–12
JB1104	12–15	JB1315	12–13
		JB1316	13–14

JB1105	20–24	

964

965 **TABLE 1.** Sample identification numbers and corresponding depth intervals of the VXE-6 pond

966 site soil pit and sediment core samples analyzed in this study.

967

968

Mineral	**Abundance (wt%)**					
	0–1 cm	**1–4 cm**	**4–7 cm**	**8–10 cm**	**12–15 cm**	**20–24 cm**
Quartz	35.6	35.2	16.6	24.9	27.9	30.7
Anorthite	30.6	31.5	23.8	30.0	32.3	37.3
Albite	7.57	9.49	4.33	6.78	7.75	5.00
Diopside	17.5	16.0	11.5	17.7	20.3	20.1
Phlogopite/muscovite	0.00	0.35	30.7	0.00	0.00	0.00
Gypsum	0.76	0.00	0.00	11.2	5.19	0.00
Bassanite	0.00	0.00	0.00	3.74	0.44	0.00
Amphibole	4.70	3.80	4.33	5.67	6.17	6.92
Clinochlore	3.34	3.75	8.68	0.00	0.00	0.00

969

970 **TABLE 2.** Mineral abundance data obtained via XRD of VXE-6 pond site soil pit samples.

971

Element	Concentration (ppm except as noted)					
	0–1 cm	**1–4 cm**	**4–7 cm**	**8–10 cm**	**12–15 cm**	**20–24 cm**
Na (wt%)	1.68	1.89	1.55	1.47	1.61	1.37
K (wt%)	1.33	1.41	2.28	1.02	1.26	0.95
Sc	18.8	18.0	20.4	17.4	17.2	17.6
Cr	111	128	106	106	96.5	103
Fe (wt%)	3.17	3.23	5.71	3.18	3.18	3.34
Co	19.1	18.6	28.8	17.9	16.9	18.0
Ni	70	71	64	44	66	62
Zn	53	55	100	55	58	60
Ga	44	19	24	40	14	43
As	<1.5	<1.7	1.33	<1.2	<0.9	<1.1
Se	<2.0	<2.1	<2.5	1.49	<2.1	<2.3
Br	<0.9	<1.1	0.3	0.3	<0.6	<0.7
Rb	45.6	51.4	116	47.8	52.9	48.7
Sr	287	296	373	274	257	238

This is the peer-reviewed, final accepted version for American Mineralogist, published by the Mineralogical Society of America.
The published version is subject to change. Cite as Authors (Year) Title. American Mineralogist, in press.
DOI: https://doi.org/10.2138/am-2022-8381. http://www.minsocam.org/

Zr	117	124	193	148	167	157
Sb	<0.1	<0.2	0.12	<0.2	<0.2	<0.1
Cs	1.09	1.30	4.68	1.08	1.24	1.21
Ba	232	259	281	202	235	190
Hf	2.67	2.60	2.98	2.87	3.35	3.22
Ta	0.35	0.44	1.13	0.72	0.78	0.82
W	<4.7	<4.7	0.9	<3.6	<2.5	<3.4
Ir (ppb)	<2.2	<2.3	<1.8	<1.5	<1.5	<1.6
Au (ppb)	<1.8	<2.9	<1.9	<1.5	0.6	<1.4
Th	4.45	4.15	12.3	4.25	5.13	5.44
U	0.72	1.29	3.42	1.40	1.11	1.20

973

974 **TABLE 3.** INAA elemental abundance data for soil pit samples from the VXE-6 pond site.

975

976

Depth (cm)	**Concentration (ppm)**									
	La	Ce	Nd	Sm	Eu	Gd	Tb	Tm	Yb	Lu
0–1	17.1	30.5	14.8	2.71	0.69	1.00	0.34	0.27	1.27	0.21
1–4	15.3	26.6	10.8	2.59	0.70	2.07	0.36	0.20	1.26	0.20
4–7	30.7	54.9	21.7	4.97	0.91	3.99	0.64	0.31	1.99	0.34
8–10	18.9	33.8	14.5	3.20	0.69	2.70	0.46	0.25	1.44	0.22
12–15	20.6	37.2	15.5	3.38	0.73	3.17	0.46	0.23	1.30	0.22
20–24	20.8	40.4	15.2	3.14	0.75	2.99	0.44	0.25	1.41	0.24

977

978 **TABLE 4.** Rare earth element data for all soil pit samples. Note: Pr, Dy, Ho, Er data not collected.

979

This is the peer-reviewed, final accepted version for American Mineralogist, published by the Mineralogical Society of America.
The published version is subject to change. Cite as Authors (Year) Title. American Mineralogist, in press.
DOI: https://doi.org/10.2138/am-2022-8381. http://www.minsocam.org/

980

Depth (cm)	**Major oxide (wt%)**							
	SiO_2	Al_2O_3	Fe_2O_3	MgO	CaO	Na_2O	K_2O	SO_3
0–1	70.8	8.07	5.27	3.81	4.76	2.19	1.27	0.29
1–4	68.3	8.94	5.22	3.82	4.95	2.11	1.40	0.10
4–7	48.5	16.2	8.25	4.53	6.27	1.76	2.88	0.49
8–10	59.1	8.29	5.11	3.35	9.83	1.79	1.61	6.70
12–15	64.3	9.15	5.39	3.65	7.46	1.93	1.51	2.94
20–24	65.7	9.75	5.41	3.44	6.55	2.05	1.58	1.48

981

982 **TABLE 5.** XRF major element chemistry data for soil pit samples from the VXE-6 pond site.

983

985

Depth (cm)	**Acid-soluble SO_4^{2-}**	
	$\delta^{34}S$ (‰)	$\delta^{18}O$ (‰)
0–1	16.7	-8.7
1–4	16.4	-8.4
4–7	15.8	-7.2
8–10	16.6	-8.9
12–15	16.2	-7.4
20–24	15.9	-7.9

986

987 **TABLE 6.** Stable isotope values of $\delta^{34}S$ and $\delta^{18}O$ in sulfate for VXE-6 soil pit samples.

988

989 FIGURE 1

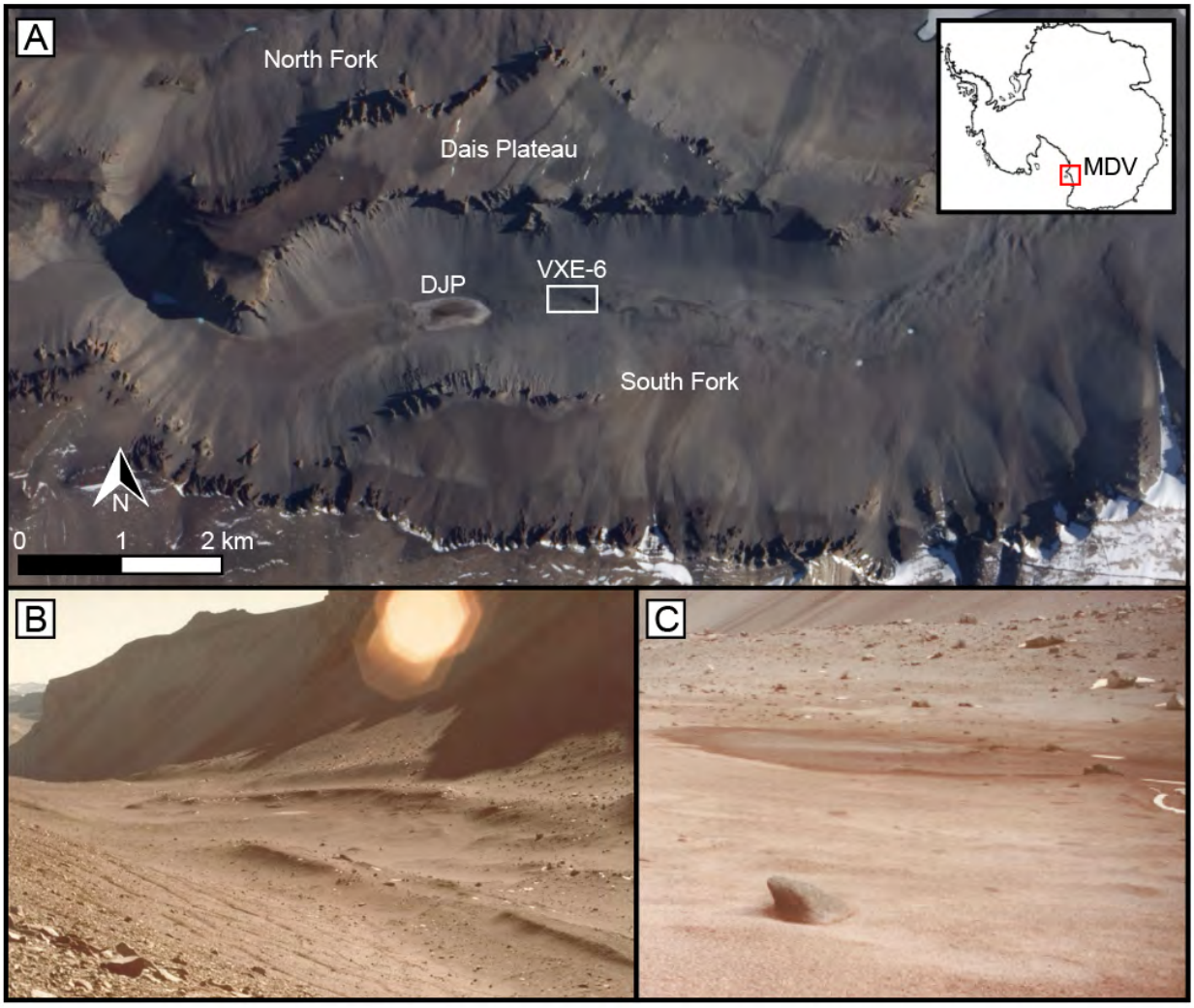

990

This is the peer-reviewed, final accepted version for American Mineralogist, published by the Mineralogical Society of America.
The published version is subject to change. Cite as Authors (Year) Title. American Mineralogist, in press.
DOI: https://doi.org/10.2138/am-2022-8381. http://www.minsocam.org/

991 FIGURE 2

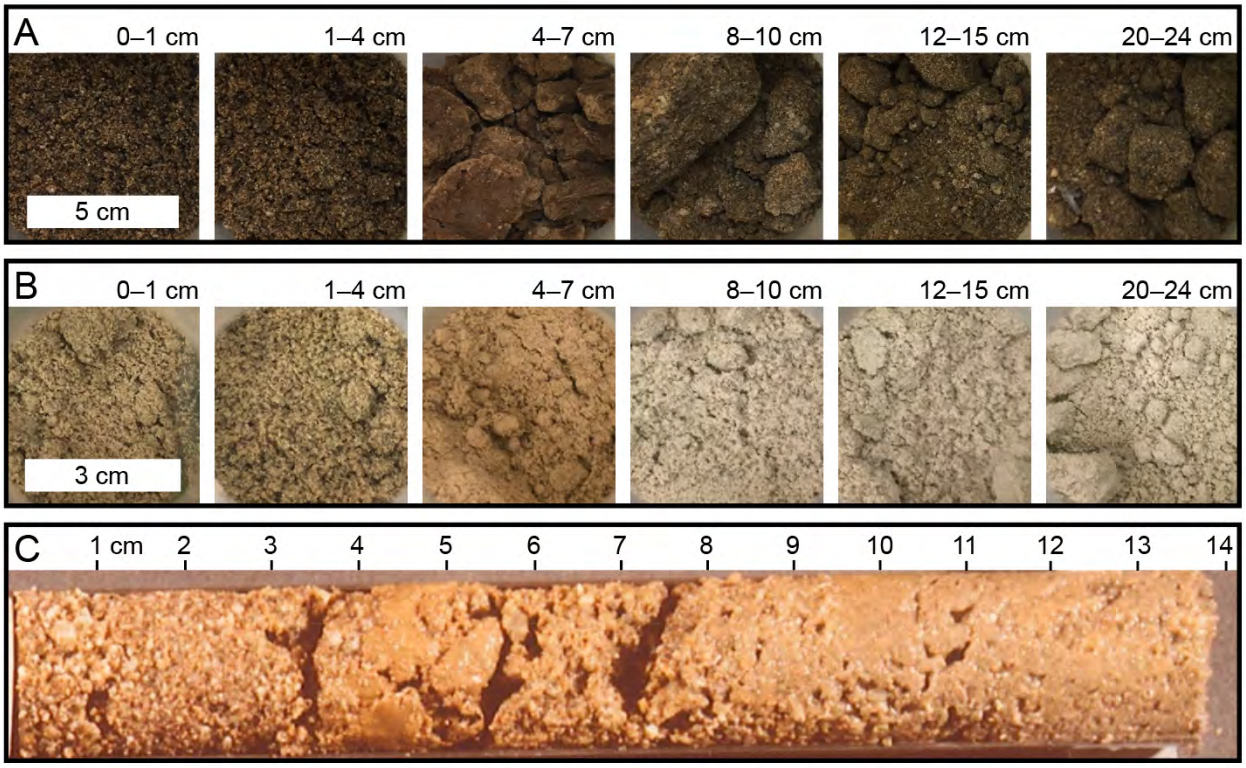

992

993 FIGURE 3

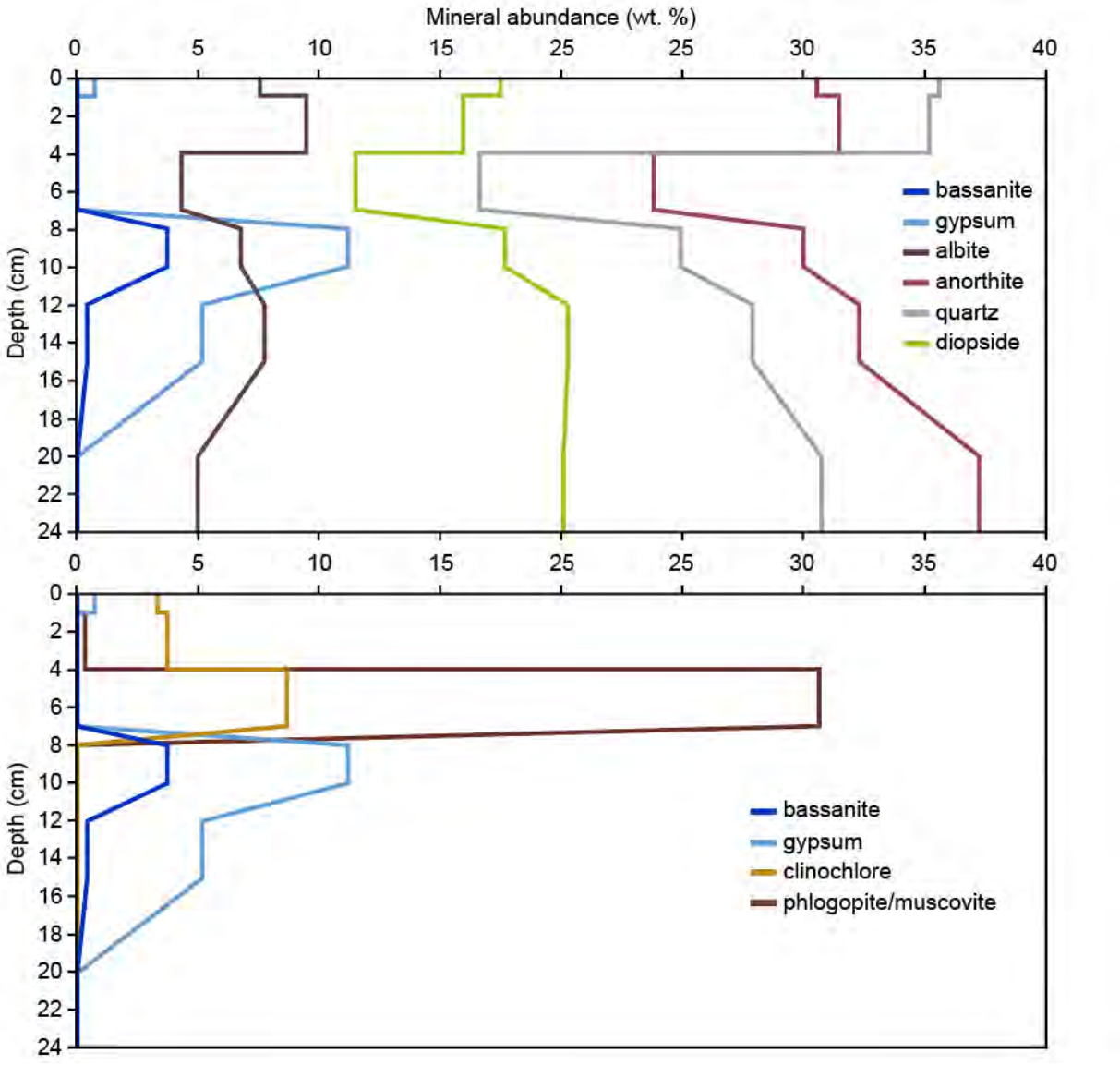

994

This is the peer-reviewed, final accepted version for American Mineralogist, published by the Mineralogical Society of America.
The published version is subject to change. Cite as Authors (Year) Title. American Mineralogist, in press.
DOI: https://doi.org/10.2138/am-2022-8381. http://www.minsocam.org/

995 FIGURE 4

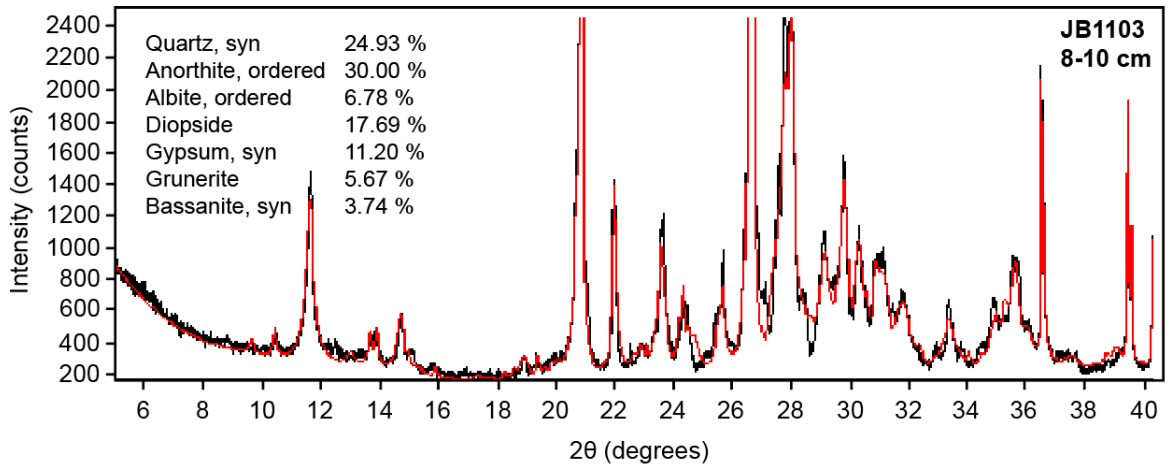

996

This is the peer-reviewed, final accepted version for American Mineralogist, published by the Mineralogical Society of America.
The published version is subject to change. Cite as Authors (Year) Title. American Mineralogist, in press.
DOI: https://doi.org/10.2138/am-2022-8381. http://www.minsocam.org/

997 FIGURE 5

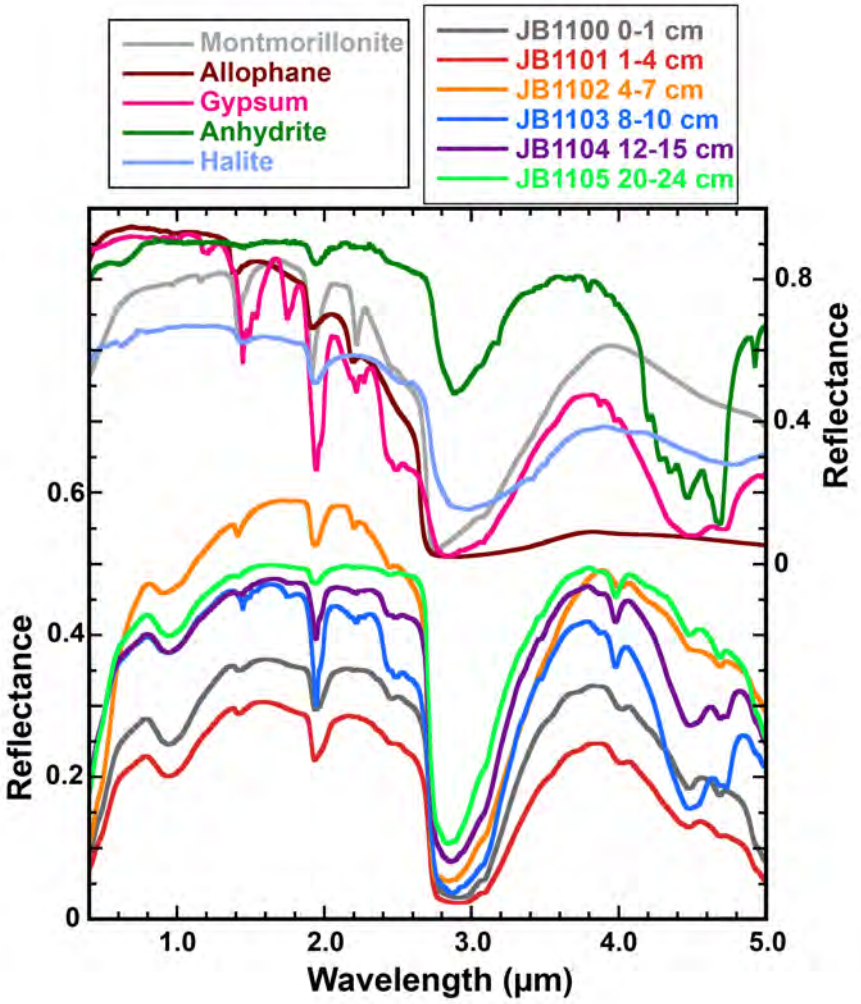

998

This is the peer-reviewed, final accepted version for American Mineralogist, published by the Mineralogical Society of America.
The published version is subject to change. Cite as Authors (Year) Title. American Mineralogist, in press.
DOI: https://doi.org/10.2138/am-2022-8381. http://www.minsocam.org/

999 FIGURE 6

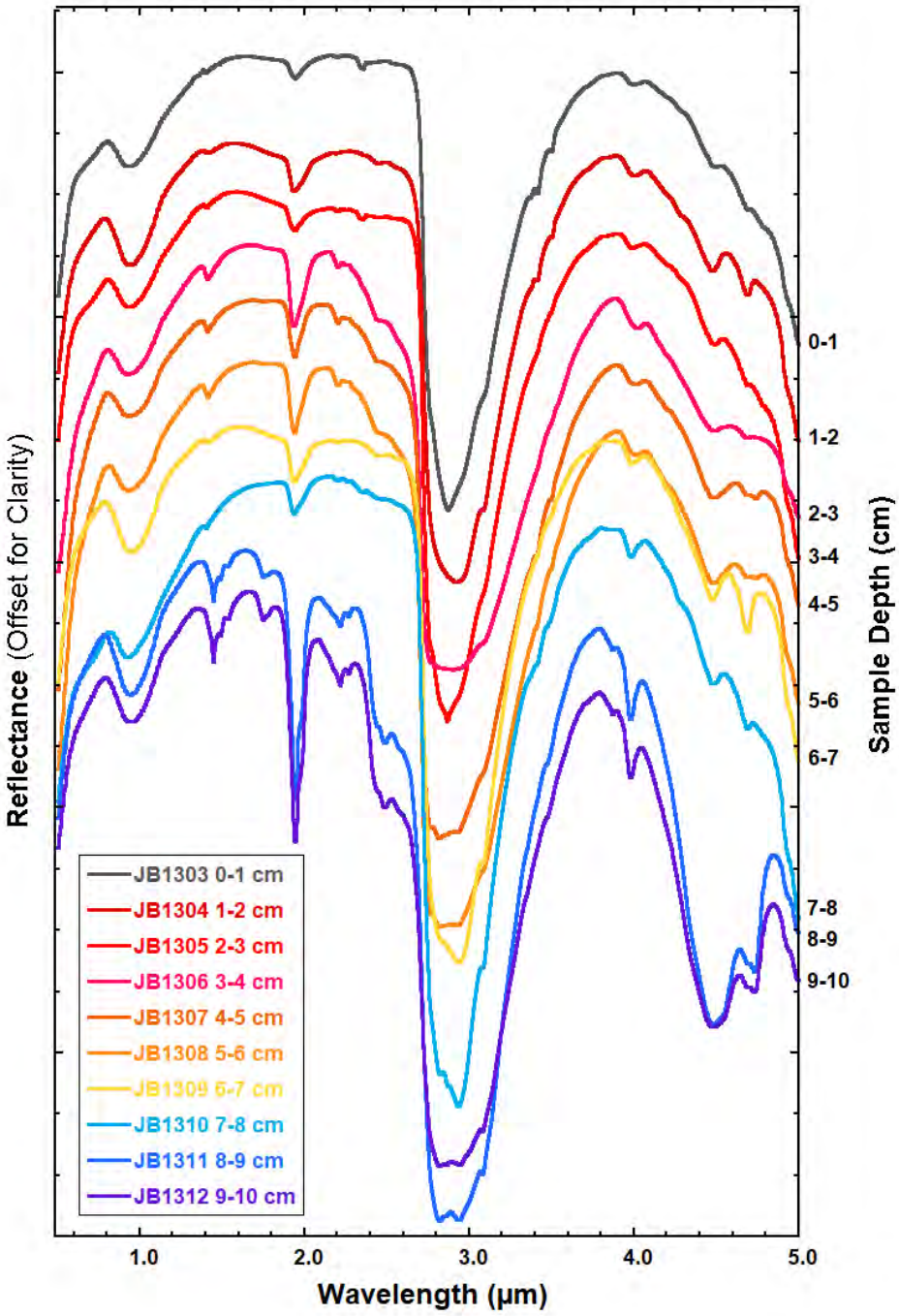

1000

This is the peer-reviewed, final accepted version for American Mineralogist, published by the Mineralogical Society of America.
The published version is subject to change. Cite as Authors (Year) Title. American Mineralogist, in press.
DOI: https://doi.org/10.2138/am-2022-8381. http://www.minsocam.org/

1001 FIGURE 7

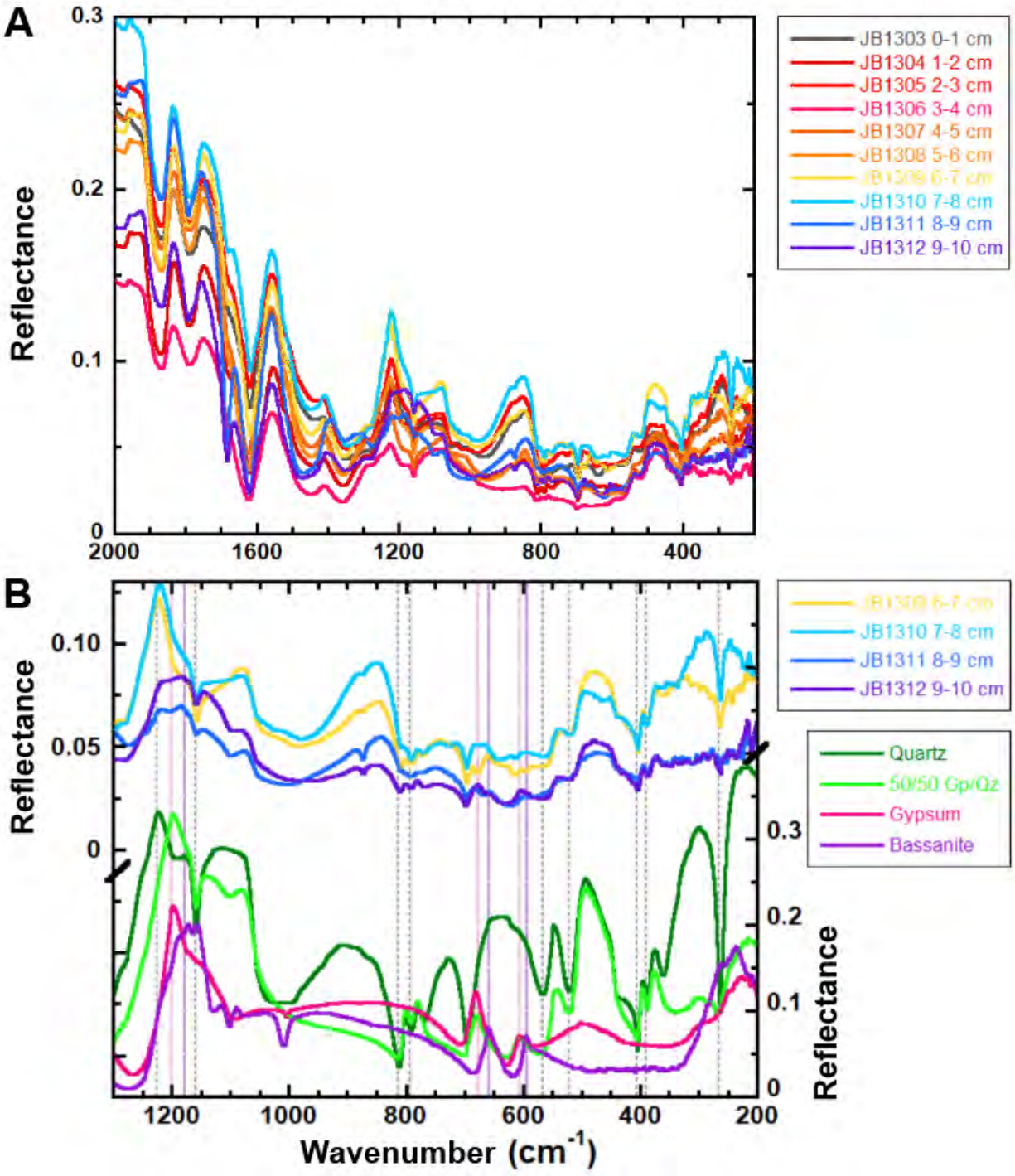

1002

This is the peer-reviewed, final accepted version for American Mineralogist, published by the Mineralogical Society of America.
The published version is subject to change. Cite as Authors (Year) Title. American Mineralogist, in press.
DOI: https://doi.org/10.2138/am-2022-8381. http://www.minsocam.org/

1003 FIGURE 8

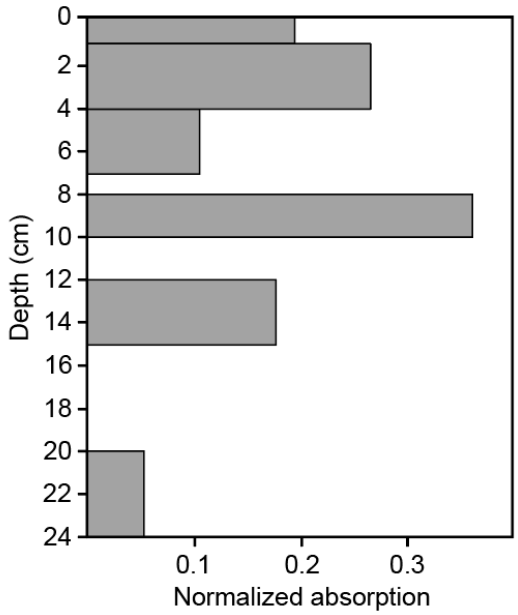

1004

This is the peer-reviewed, final accepted version for American Mineralogist, published by the Mineralogical Society of America.
The published version is subject to change. Cite as Authors (Year) Title. American Mineralogist, in press.
DOI: https://doi.org/10.2138/am-2022-8381. http://www.minsocam.org/

1005 FIGURE 9

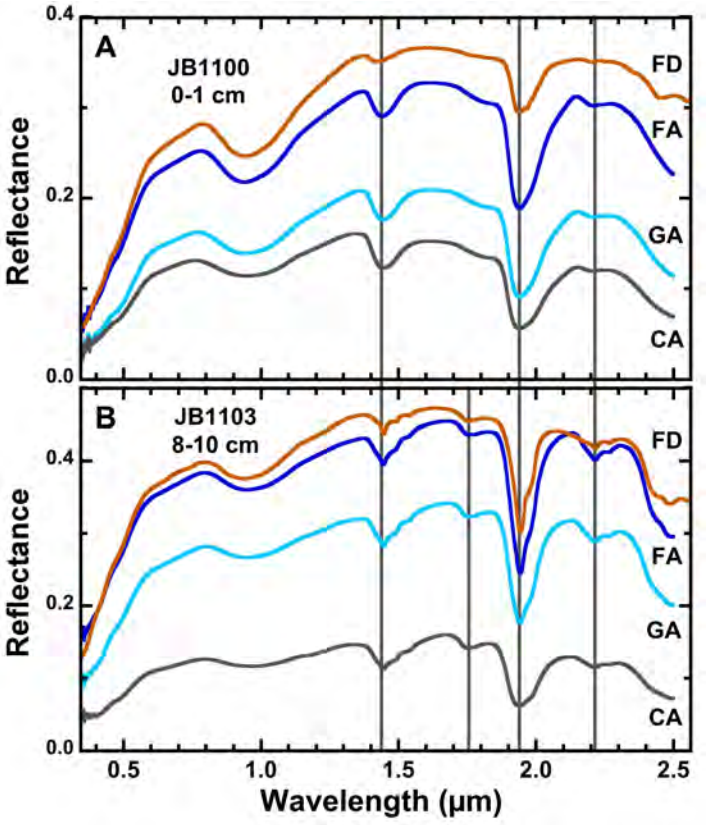

1006

This is the peer-reviewed, final accepted version for American Mineralogist, published by the Mineralogical Society of America.
The published version is subject to change. Cite as Authors (Year) Title. American Mineralogist, in press.
DOI: https://doi.org/10.2138/am-2022-8381. http://www.minsocam.org/

1007 FIGURE 10

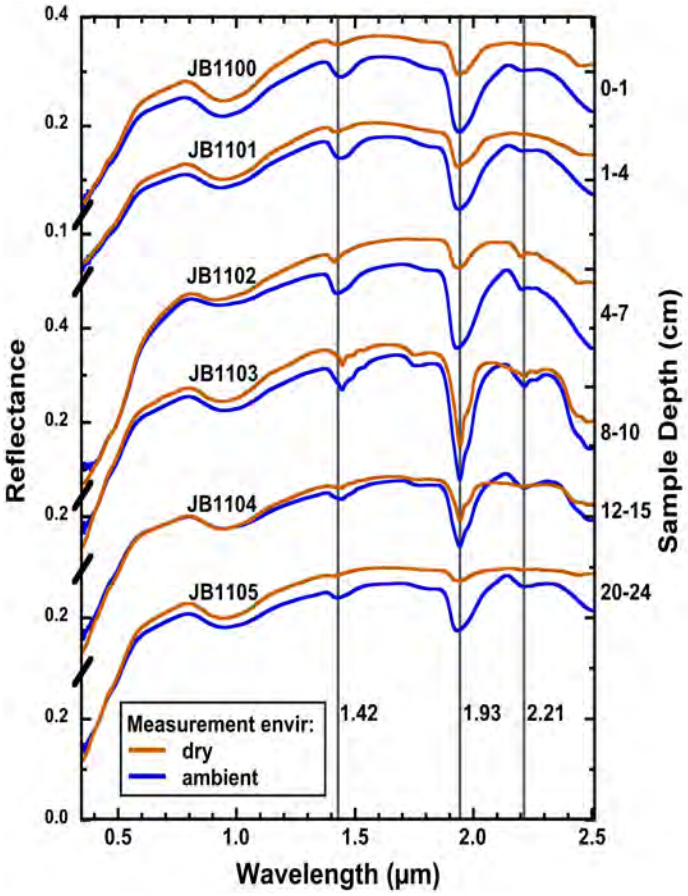

1008

This is the peer-reviewed, final accepted version for American Mineralogist, published by the Mineralogical Society of America.
The published version is subject to change. Cite as Authors (Year) Title. American Mineralogist, in press.
DOI: https://doi.org/10.2138/am-2022-8381. http://www.minsocam.org/

1009 FIGURE 11

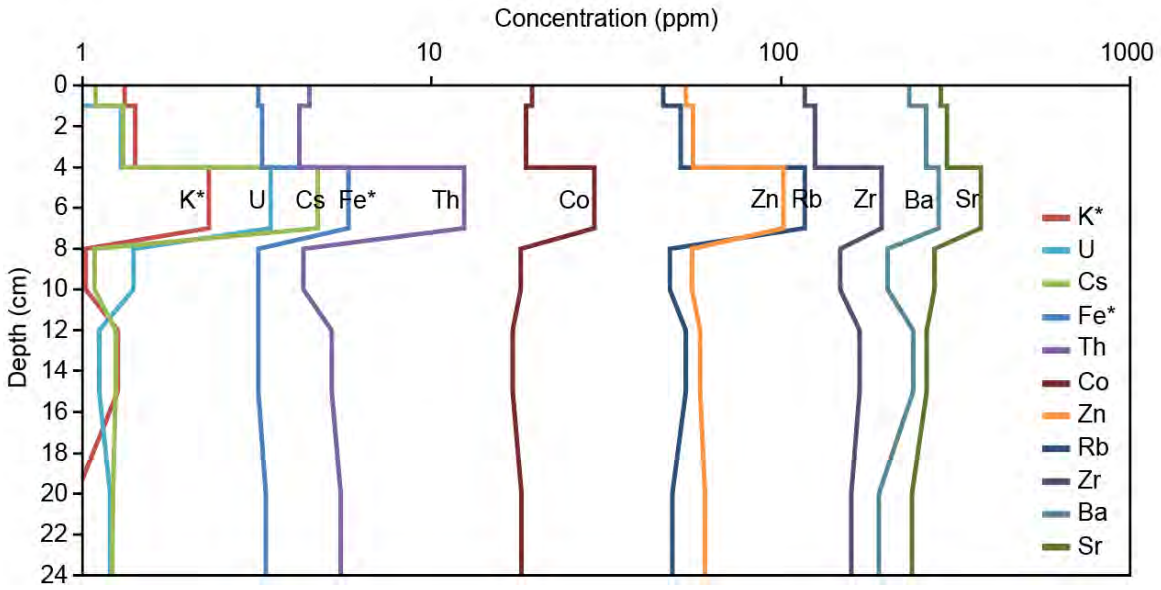

1010

1011 FIGURE 12

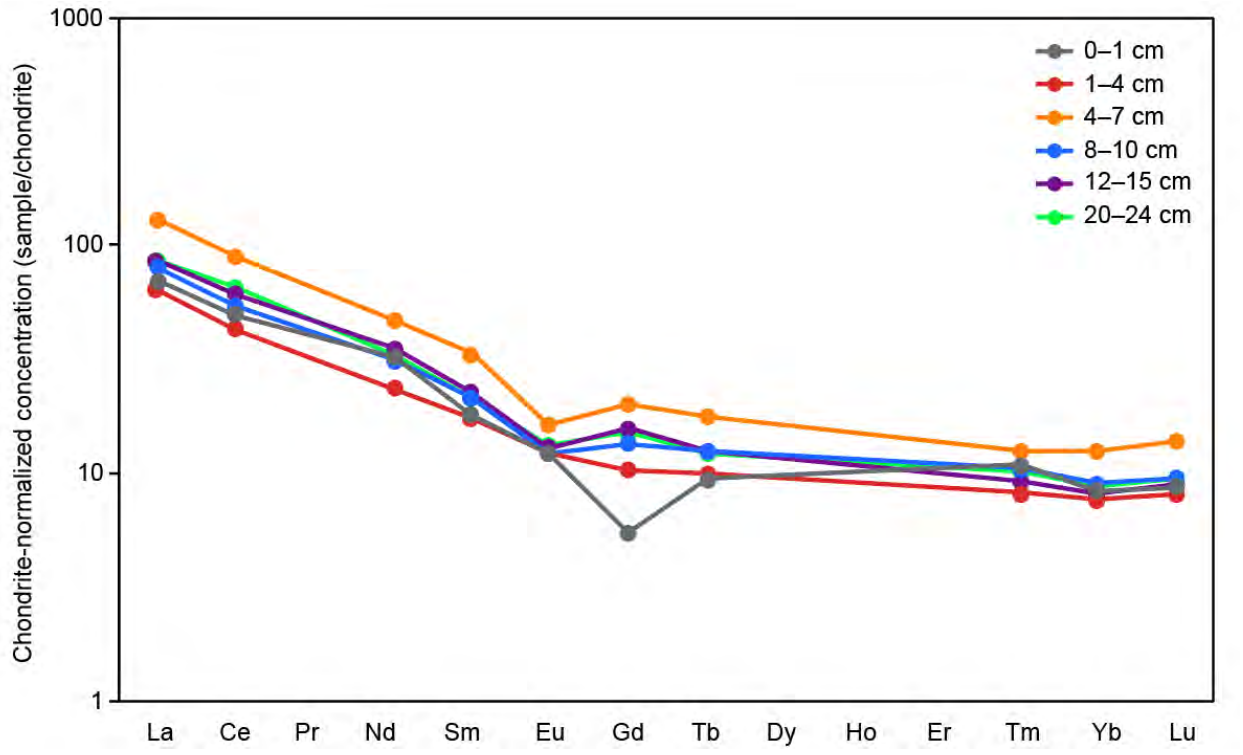

1012

This is the peer-reviewed, final accepted version for American Mineralogist, published by the Mineralogical Society of America.
The published version is subject to change. Cite as Authors (Year) Title. American Mineralogist, in press.
DOI: https://doi.org/10.2138/am-2022-8381. http://www.minsocam.org/

1013 FIGURE 13

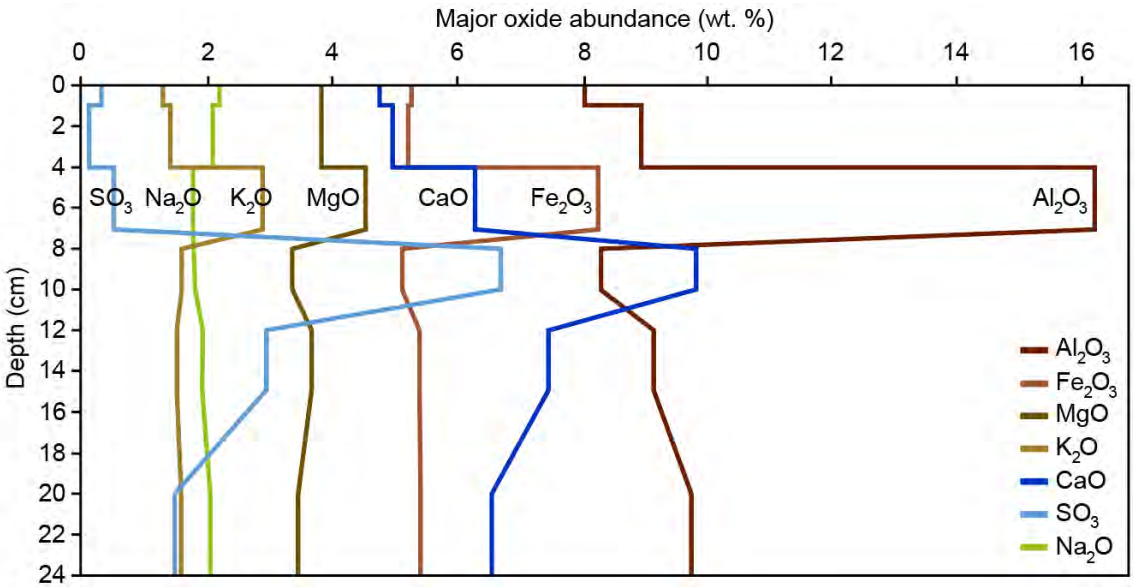

1014

1015

This is the peer-reviewed, final accepted version for American Mineralogist, published by the Mineralogical Society of America.
The published version is subject to change. Cite as Authors (Year) Title. American Mineralogist, in press.
DOI: https://doi.org/10.2138/am-2022-8381. http://www.minsocam.org/

1016 FIGURE 14

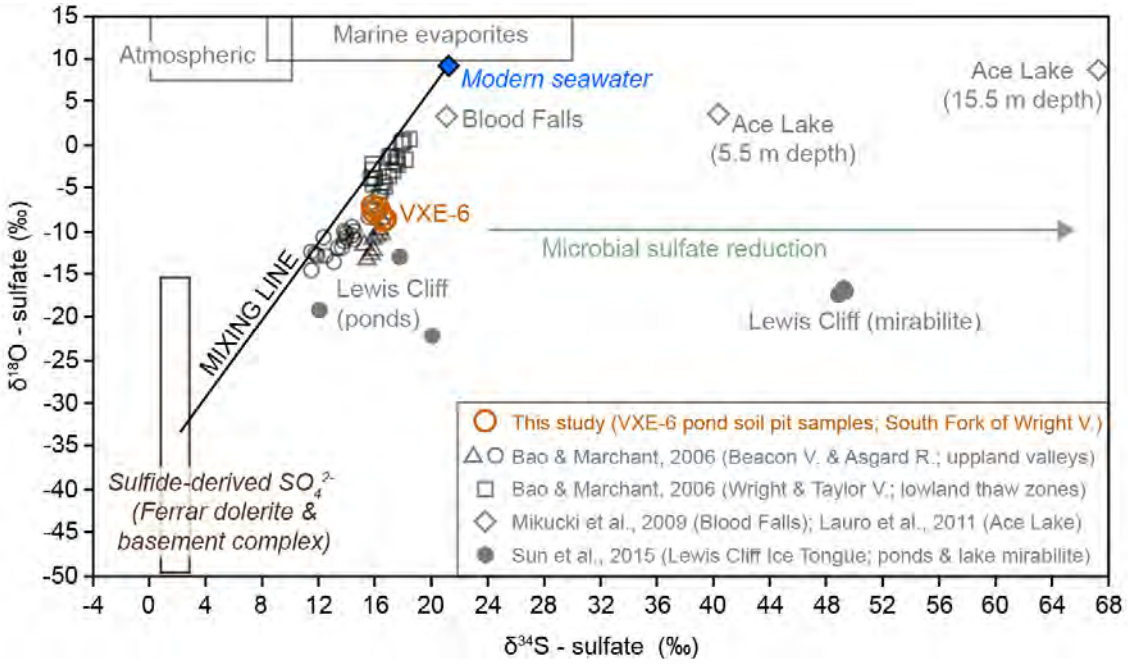

1017

This is the peer-reviewed, final accepted version for American Mineralogist, published by the Mineralogical Society of America.
The published version is subject to change. Cite as Authors (Year) Title. American Mineralogist, in press.
DOI: https://doi.org/10.2138/am-2022-8381. http://www.minsocam.org/

1018 FIGURE 15

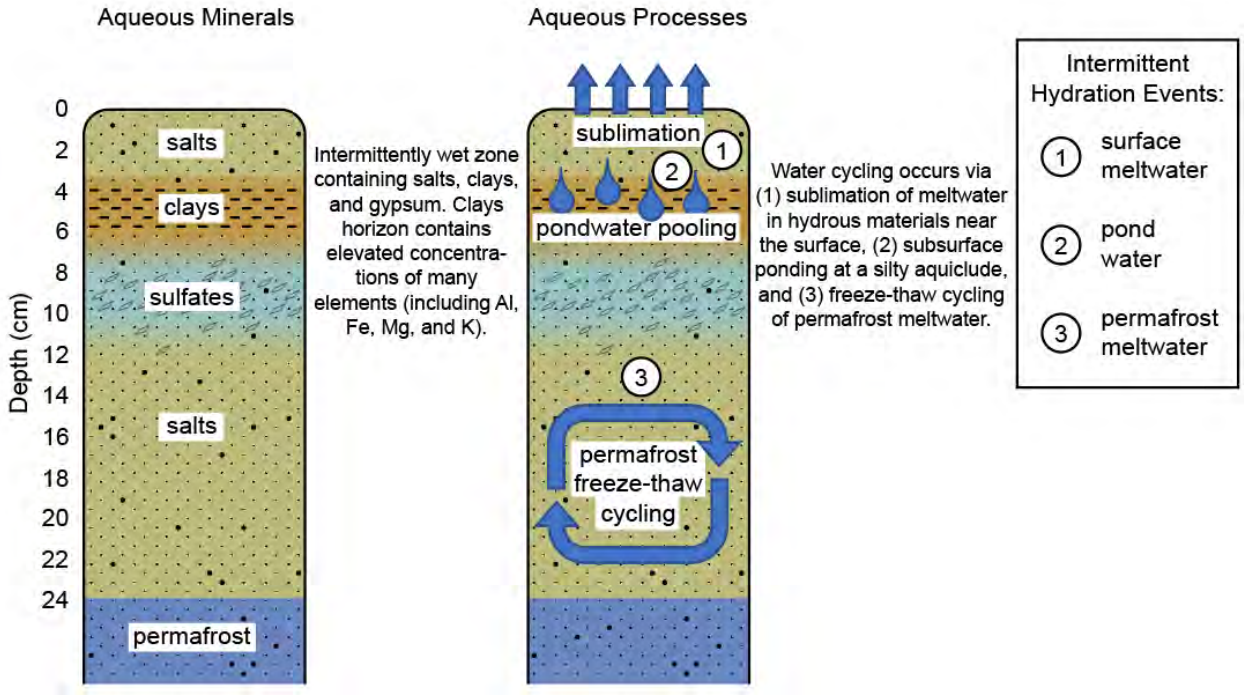

1019